Transient heat loss of hot water tanks using CFD

Master's thesis in Sustainable Energy Systems

LINNÉA TOBIASSON

DEPARTMENT OF MECHANICS AND MARITIME SCIENCES

CHALMERS UNIVERSITY OF TECHNOLOGY
Gothenburg, Sweden 2025
www.chalmers.se

Master's thesis 2025

Transient heat loss of hot water tanks using CFD

LINNÉA TOBIASSON

CHALMERS
UNIVERSITY OF TECHNOLOGY

Department of Mechanics and Maritime Sciences
Division of Fluid Dynamics
Chalmers University of Technology
Gothenburg, Sweden 2025

Transient heat loss of hot water tanks using CFD
LINNÉA TOBIASSON

Supervisor: Alexander Lindblom, NIBE AB
Examiner: Lars Davidson, Department of Mechanics and Maritime Sciences

Master's Thesis 2025
Department of Mechanics and Maritime Sciences
Division of Fluid Dynamics
Chalmers University of Technology
SE-412 96 Gothenburg
Telephone +46 31 772 1000

Typeset in LaTeX
Printed by Chalmers Reproservice
Gothenburg, Sweden 2025

Transient heat loss of hot water tanks using CFD
LINNÉA TOBIASSON
Department of Mechanics and Maritime Sciences
Chalmers University of Technology

Abstract

The product development process can be a time consuming process. A computational fluid dynamics (CFD) software can be used to shorten the design cycle, as well as lower the material waste used for experimental tests. CFD is the numerical method of predicting fluid behavior. It can solve a large variety of different complex problems, though, one of its drawbacks is the more numerical accurate solution the higher computational cost. This thesis focuses on developing a methodology that keeps the computational cost to a minimum while simultaneously provide results that correlate to experimental data of unsteady state simulations, also called transient CFD simulations.

The methodology was conducted through a literature analysis, analytical calculations and evaluated by being tried out on two simulations using the CFD software STAR-CCM+. The numerical results were compared to experimental data gathered from an experimental test called standing heat-loss test, performed on a thermal energy storage (TES) tank with and without insulated surfaces. The literature analysis suggested a numerical setup using the Boussinesq approximation with fully coupled modeling and an implicit time-stepping approach. The analytical calculations gave an initial value on the convection boundary condition (BC), they also indicated to use different heat transfer coefficients on different heights of the uninsulated tank, while a constant heat transfer coefficient can be used for the insulated tank.

A common approach to reduce the computation time is to decrease the domain size by using symmetry planes. Symmetry planes can however disrupt fluid flow and alter the numerical results. To remove any uncertainties of a reduced domain size it is advised to do a comparison between the results from the whole domain and the reduced size. In these simulations it could be observed that the symmetry planes caused instability of the solver in more turbulent flow regions but no other differences could be seen. A multi-time-stepping approach combined with a minimum convergence criterion of 10^{-6} gave the best reduction of computation time while providing results that correlated to experimental data. This approach however varies greatly from case to case and as larger time-steps approximates solutions this approach is not suggested if the goal is to have simulations with numerical independence.

With all time reducing strategies implemented, the simulations could be reduced from 700 cores, 48 hours to 4 cores and 1 hour.

Keywords: Heat transfer, Natural convection, Buoyancy, Thermal Energy Storage, Water tank, Transient CFD simulation, STAR-CCM+.

Acknowledgements

This master's thesis was conducted as part of the Master of Science program in Mechanical Engineering at Chalmers University of Technology. The work was carried out during the spring of 2025 at NIBE Trollhättan.

Many thanks to NIBE!

I am very grateful to have been given the opportunity to write this thesis. Thank you to everyone in the Trollhättan office for creating a welcoming and supportive environment.

A sincere thank you to my examiner, Professor Lars Davidson. I cannot thank you enough for your support and academic guidance during this spring.

Finally, a thousand times thank you to my family and to everyone who has encouraged and supported me throughout my academic journey.

Linnéa Tobiasson, Gothenburg, June 2025

Notations and Acronyms

C_p	Specific Heat Capacity at Constant Pressure	$\mathrm{J/(kg \cdot K)}$
ρ	Density	$\mathrm{kg/m^3}$
μ	Dynamic viscosity	$\mathrm{Pa \cdot s}$
ν	Kinematic viscosity	$\mathrm{Pa \cdot s}$
κ	Thermal conductivity	$\mathrm{W/(m \cdot K)}$
T	Static temperature	K
p	Pressure	Pa
g	Gravitational acceleration	$\mathrm{m/s^2}$
t	Physical time	s
α	Thermal diffusivity	$\mathrm{m/s^2/s}$
r	Radius	m
H	Height	m
L	Characteristic length	m
Ra	Rayleigh number	$-$
Pr	Prandtl number	$-$
Re	Reynolds number	$-$
Nu	Nusselt number	$-$
L	Characteristic length	m
β	Volume expansion coefficient	$-$
R	Thermal resistance	$\mathrm{K/(W)}$
h	Heat transfer coefficient	$\mathrm{W/(m^2 \cdot K)}$
U	Overall heat transfer coefficient	$\mathrm{W/(m^2 \cdot K)}$

BC	Boundary Condition
BDF	Backward Differentiation Formula
CAD	Computer-aided design
CFD	Computational Fluid Dynamics
CPU	Central Processing Unit
FVM	Finite Volume Method
PDE	Partial Differential Equations
PUR	Polyurethane
TES	Thermal Energy Storage

Contents

List of Figures

List of Tables

1
Introduction

1.1 Background

The product development process can be a time consuming process [1]. A computational fluid dynamics (CFD) software can be used to shorten the design cycle as well as reducing material waste used in experimental tests [2]. CFD is the numerical method of predicting fluid behavior and its interaction with the surrounding environment [3]. CFD can solve complex problems by coupling the physics of fluids with other areas of interest such as, heat transfer, aero-acoustics or electrochemistry [4]. Though, one of its drawbacks is the more numerical accurate solution the higher computational cost and finding a solution that represent the experimental data is often an iterative process. It is therefore desirable to have a strategy of how to produce reliable results without using an excessive amount of resources. This is especially important with large simulations such as unsteady simulations where the physical properties varies in both space and time [2]. This thesis focuses on a methodology for unsteady CFD simulations. The goal is to find a robust method that can be used for several different problems, as well as keeping the computational cost to a minimum while simultaneously provide results that correlate to experimental data.

1.2 Problem Specification

The methodology is to be developed through a literature analysis, analytical calculations and evaluated by being tried out on two simulations using the CFD software STAR-CCM+. The numerical results are going to be compared to experimental data gathered from an experimental test called standing heat-loss test performed on a thermal energy storage (TES) tank with and without insulated surfaces. The tank is to be combined with a heat pump where the tank stores hot water to improve pump efficiency. The experimental test is conducted by continuously measuring the temperature in the water while the hot water stored in the tank cools down without interruption. The surrounding air is stagnant and so, the heat transfer is driven by natural convection. As heat is lost to the surrounding air the hot water elements flows to the top and the cooler falls to the bottom of the tank due to density differences and buoyancy. With time, a temperature layering called thermal stratification appears, where an insulated tank does not have as of a distinct temperature layering due to the decreased rate of heat loss.

Similar studies on hot water tanks has been performed before. Lago *et al.*, propose that simulations in 1D do not capture the details of buoyancy and thermal satisfaction [5], and for a more detailed and accurate solution a 3D approach is recommended. Savicki *et al.*, has conducted both static and dynamic CFD simulations of hot water tanks [6]. Their numerical setup included the Boussinesq approximation with fully coupled modeling and an implicit time stepping approach. They used a smaller time step of 0.5 seconds for simulations with higher fluid flow together with a minimum convergence criterion of 10^{-6} to converge each time step. To decrease the computation time, they carried out simulations on a smaller geometry and hence domain size. Their domain size was 1/4 of the physical geometry when the flow was slower and 1/2 when the fluid flow was higher and more turbulent.

1.2.1 Purpose

The purpose with this thesis is to give advise and suggestions of how to achieve a well thought out starting point to carry out resource heavy simulations such as transient CFD simulations. A well initial setup will minimize the number of simulation runs to satisfy correlation between numerical and physical results. This will both make it possible to achieve reliable numerical results faster, the product development process can be shortened and this will in turn reduce total costs. In the thesis it will be a discussion of how to decide boundary condition, define the time-marching approach and how different stopping criteria impact the results. There will also be a discussion about how trustworthy the results are if symmetry planes are used to decrease the size of the domain.

1.2.2 Aim

The aim of this work is to develop a robust method for conducting unsteady CFD simulations, with a particular focus on reducing computation time while maintaining correlation to experimental data.

1.2.3 Limitations

1. All CFD simulations will be done in 3D due to the complexity of mixing, buoyancy effects and thermal stratification in the water tank.
2. The design of the tank is fixed and focus will only be given on optimizing the method to achieve correlation with experimental data and reduce computational resources.
3. Due to the projects duration of 20 weeks and the limited computer power, a prioritization of the simulation is to be performed and justified through a literature analysis.

2
Theory

2.1 Heat Transfer

Heat transfer is the transfer of thermal energy due to temperature differences. Heat transfers in three ways, convection, conduction and radiation.

2.1.1 Convection

Convection is heat transported due to a movement of a fluid or gas. Convection is the sum of diffusion and advection of a fluid. The rate of cooling by convection is described by Newton's law of cooling seen in eq. (2.1). h is the heat transfer coefficient, A is the surface area and ΔT is the temperature difference between the surface and bulk fluid.

$$q = hA\Delta T \tag{2.1}$$

2.1.2 Natural Convection

Convection can be forced or natural. Forced convection is heat transfer with external means and natural convection without external means.

Natural convection starts from a temperature gradient that generate density differences and buoyancy. The gravitational force per unit of volume ρg is acting downwards on each fluid element. The gravitational force is often divided into a buoyancy term $(\rho - \rho_\infty)g$ and a hydrodynamic term $\rho_\infty g$.

If the density ρ solely varies due to temperature changes, the volumetric thermal expansion coefficient β can be simplified to:

$$\beta \approx -\frac{1}{\rho}\frac{\Delta\rho}{\Delta T} = -\frac{1}{\rho}\frac{\rho_\infty - \rho}{T_\infty - T} \tag{2.2}$$

This can be rearranged as (2.3), which is a simplification called the Boussinesq approximation.

$$(\rho_\infty - \rho) \approx \rho\beta\,(T - T_\infty) \tag{2.3}$$

2.1.2.1 The Boundary Layer of Natural Convection

Natural convection of a vertical cylinder can be treated as a vertical plate when the curvature of a vertical cylinder meet the criteria of:

$$\frac{D}{L} \geqslant \frac{35}{Gr^{1/4}} \tag{2.4}$$

Rayleigh number seen in (2.5) explain the flow behavior of the boundary layer in natural convection cases. g is the gravitational acceleration, β is the volume expansion coefficient. L is the characteristic length (the characteristic length is the height of a vertical cylinder). ν is kinematic viscosity coefficient and α is the thermal diffusivity.

$$Ra = \frac{g\beta\Delta TL^3}{\nu\alpha} \tag{2.5}$$

The Rayleigh number can also be expressed as a product of Grashof number and Prandtl number. Grashof number (2.6) is the ratio of the buoyancy force to the viscous force.

$$Gr = \frac{g\beta\Delta TL^3}{\nu^2} = \frac{Buoyancy\ force}{Viscous\ force} \tag{2.6}$$

Prandtl number (2.7) is a dimensionless number of momentum diffusivity and thermal diffusivity.

$$Pr = \frac{\nu}{\alpha} = \frac{\mu\, Cp}{\kappa} \tag{2.7}$$

Nusselt number in (2.8) is used in laminar natural convection and (2.9) in turbulent natural convection.

$$Nu = \begin{cases} 0.53Ra^{1/4}, & \text{if } 10^4 \leq Ra \leq 10^9 \quad (2.8) \\ 0.1Ra^{1/3}, & \text{if } 10^9 \leq Ra \leq 10^{13} \quad (2.9) \end{cases}$$

The Nusselt number can also be expressed for the entire range as:

$$Nu = \left\{ 0.825 + \frac{0.387Ra^{1/6}}{\left[1 + (0.492/Pr)^{9/16}\right]^{8/27}} \right\}^2 \tag{2.10}$$

The heat transfer coefficient h can be calculated from the Nusselt number Nu, the thermal conductivity of the fluid k and the characteristic length of the geometry L:

$$h = \frac{Nu\, k}{L} \tag{2.11}$$

The thermal resistance of convection R is the inverse of of heat transfer coefficient and surface area:

$$R = \frac{1}{hA} \tag{2.12}$$

The boundary layer thickness with a temperature profile of a vertical heated plate with laminar convection is shown in figure 2.1. Both the velocity of the air and the boundary layer thickness increase with plate height. The temperature of the air close to the hot plate is equal to the plate temperature and decreases with increased distance from the plate until it is equal to the temperature of ambient air.

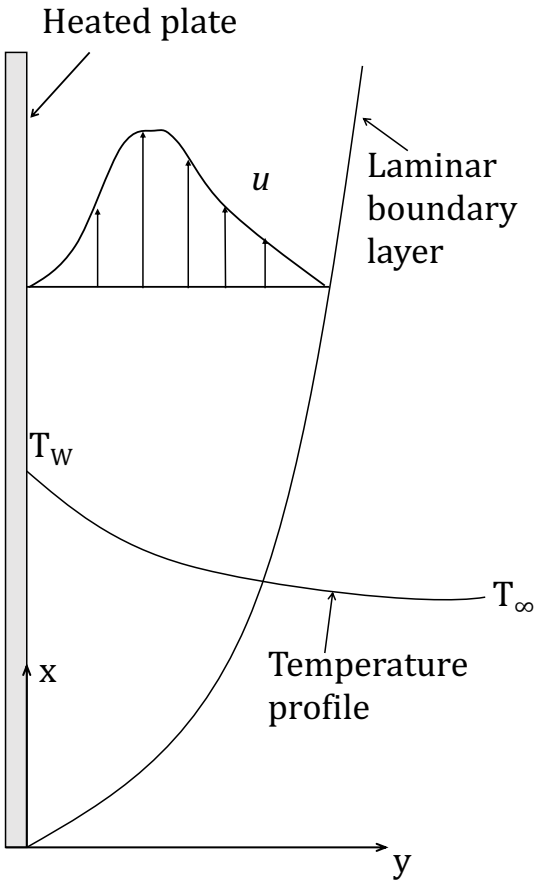

Figure 2.1: Laminar boundary layer thickness of a heated vertical plate [7]

2.1.3 Conduction

Thermal conduction is governed by Fourier's law (2.13). Heat is transferred through a solid or fluid. Different materials or mediums has different ability to transfer heat. This is explained by the the material property thermal conductivity, k. dx is the thickness of the element and dT is the temperature difference of the two sides.

$$q = -kA\frac{dT}{dx} \tag{2.13}$$

2.1.3.1 Metals and Alloys

The electrons in metals are carriers of electricity and heat [8]. Metals have a large number of free electrons that are not bound to one position and hence metals are often a good electrical- and heat conductor. Alloys are a mixture of one or several metals with other element or elements. Steel, bronze and stainless steel are a few examples of alloys. An increase in temperature increase the thermal conductivity of the alloy.

2.1.3.2 Heat-Insulating Materials

Heat insulating materials have low thermal conductivity. Materials used for insulation have a conductivity of 0.25 W/mK or lower [8]. The heat insulating materials have no free electrons, and the heat is solely transferred through vibrations of the atoms. Heat insulating materials have discontinuous porosity and the thermal conductivity depend on the material density. A higher density improve thermal conductivity due to a decreased amount of air trapped in the material. Air has poor heat conductivity compared to the solid material.

2.1.4 Radiation

Radiation is heat transferred from all matter through electromagnetic waves. The equation for thermal radiation is seen in (2.14). σ is the Stefan–Boltzmann constant, ε is the emissivity, and T_1 is the static temperature of the geometry surface in Kelvin and T_2 is the temperature of surrounding surface in Kelvin. Heat transfer by radiation has a strong correlation to the temperature of the surfaces. Heat transfer through radiation can vary significantly due to if the material has been prepared with a reflective coating [9].

$$q = \varepsilon\sigma(T_1^4 - T_2^4) \tag{2.14}$$

2.2 Fluid Dynamics

Continuum assumption state that instead of treating each molecule on its own it is assumed that the whole fluid varies with temperature, density and pressure. The continuum assumption can be applied to most fluid mechanics applications and fluids can then be treated as continuous and mathematically formulated as partial differential equations (PDE).

2.2.1 Conservation of Mass, Momentum, and Energy

Conservation of mass, momentum, and energy are fundamental concepts of physics. The continuity equation (2.1) is the mathematical expression of conservation of mass in a system. The momentum equations (2.2), (2.3), and (2.4) explain that momentum is constant in a closed system. The energy equation (2.5) is the mathematical representation of the law of conservation of energy.

Continuity Equation, Incompressible Flow:

$$\nabla \cdot \vec{v} = 0 \tag{2.1}$$

The momentum equations are governed by the Navier-Stokes Equations. Below is the governing equations for incompressible flow in Cartesian coordinates in x,y,z-direction.

Momentum Equation, $x - direction$:

$$\rho\left(\frac{\partial u}{\partial t} + u\frac{\partial u}{\partial x} + v\frac{\partial u}{\partial y} + w\frac{\partial u}{\partial z}\right) = -\left(\nabla P\right)_x + \rho g_x + \mu\left(\nabla^2 u\right) \tag{2.2}$$

Momentum Equation, $y - direction$:

$$\rho\left(\frac{\partial v}{\partial t} + u\frac{\partial v}{\partial x} + v\frac{\partial v}{\partial y} + w\frac{\partial v}{\partial z}\right) = -\left(\nabla P\right)_y + \rho g_y + \mu\left(\nabla^2 v\right) \tag{2.3}$$

Momentum Equation, $z - direction$:

$$\rho\left(\frac{\partial w}{\partial t} + u\frac{\partial w}{\partial x} + v\frac{\partial w}{\partial y} + w\frac{\partial w}{\partial z}\right) = -\left(\nabla P\right)_z + \rho g_z + \mu\left(\nabla^2 w\right) \tag{2.4}$$

The energy equation (2.5) is the mathematical expression of conservation of energy. The law of conservation of energy state that energy can not be destroyed, it can only be transformed from one form to another. The energy equation for thermal analysis is governed by the first law of thermodynamics, and include kinetic energy, potential energy and internal energy.

Energy equation:

$$\rho c_p\left(\frac{\partial T}{\partial t} + \vec{v} \cdot \nabla T\right) = \nabla \cdot (k \nabla T) \tag{2.5}$$

2.2.2 Laminar and Turbulent Flow

Reynolds number (2.6) describe the flow behavior. Reynolds number is the ratio of inertia to viscous forces. The flow is laminar for low Reynolds number and turbulent for high Reynolds number.

$$Re = \frac{\rho \cdot u \cdot L}{\mu} = \frac{u \cdot L}{\nu} \tag{2.6}$$

2.3 CFD

Simcenter STAR-CCM+ discretize the partial derivatives numerically with the finite volume method (FVM). The governing equations varies depending on the type of problem.

2.3.1 Governing Equations for Buoyancy-Driven Flow

Natural convection problems are typically solved with governing equations for buoyancy driven flows [4]. For larger temperature differences a varying density approach is suggested to capture the larger density differences in the fluid. Problems with smaller temperature differences can be solved with an numerical approximation of constant density and gravitational force. This approximation is called the Boussinesq approximation and is typically less computational heavy than using varying density of the flow physics.

2.3.1.1 Varying Density Approach

The polynomial density approach uses a mathematical expression for a flow with variable-density $\rho = \rho(T)$.

Continuity Equation, Incompressible Flow:

$$\frac{\partial \rho}{\partial t} + \nabla \cdot (\rho \vec{u}) = 0 \tag{2.1}$$

Momentum Equation, $x, y, z - direction$:

$$\rho \left(\frac{\partial \vec{u}}{\partial t} + \vec{u} \cdot \nabla \vec{u} \right) = -\nabla p + \nabla \cdot (\mu \left(\nabla \vec{u} + (\nabla \vec{u})^T \right) - \frac{2}{3} \mu (\nabla \cdot \vec{u}) \mathbf{I}) + \rho \vec{g} \tag{2.2}$$

Energy Equation:

$$\rho c_p \left(\frac{\partial T}{\partial t} + \vec{u} \cdot \nabla T \right) = \nabla \cdot (k \nabla T) + \Phi \tag{2.3}$$

2.3.1.2 The Boussinesq Approximation

The governing equations are written in three dimensions with Cartesian coordinates and solved taking into account the following assumptions: Unsteady state, laminar flow, constant water density with the exception of varying linearly in the buoyancy term. The equations are coupled and should be solved simultaneously.

Continuity Equation, Incompressible Flow:

$$\nabla \cdot \vec{v} = 0 \tag{2.4}$$

Momentum Equation, $x, y, z - direction$:

$$\frac{\partial \mathbf{u}}{\partial t} + (\mathbf{u} \cdot \nabla)\mathbf{u} = -\frac{1}{\rho_0}\nabla p + \nu \nabla^2 \mathbf{u} + \mathbf{g}\,\beta(T - T_\infty) \tag{2.5}$$

Energy Equation:

$$\frac{\partial T}{\partial t} + \vec{v} \cdot \nabla T = \alpha \nabla^2 T \tag{2.6}$$

2.3.2 The Coupled Flow Solver

The conservation equations of mass and momentum can be solved with a coupled or segregated approach. The coupled flow model solves the conservation equations of mass and momentum simultaneously while the segregated flow model solves equations sequentially. The coupled flow model used together with the coupled energy model are suited for compressible flows and flows with a dominant source term, e.g. buoyancy.

2.3.3 Time-Marching Approach

The coupled flow solver use a pseudo-time-marching approach to solve the unsteady term of the governing equations. This term can be solved with a implicit or explicit integration scheme.

With the unsteady implicit approach (2.7) a defined number of inner iterations are solved to converge the solution for each defined time-step. The inner iterations can be of implicit spatial integration or explicit spatial integration schemes. The Courant number is used in the calculation of optimal pseudo-time-steps.

$$\begin{gathered} Q^{(0)} = Q_n \\ \left[\Gamma + \tfrac{3}{2}\tfrac{\Delta\tau}{\Delta t}\tfrac{\partial W}{\partial Q}\right]\Delta Q = \Delta\tau\left\{R^{(i-1)} + \tfrac{1}{2\Delta t}\left(3W^{(i-1)} - 4W^{(n)} + W^{(n-1)}\right)\right\} \\ Q_{n+1} = Q^{(m)} \end{gathered} \tag{2.7}$$

With the unsteady explicit approach the same physical time-step is used for all cells in the domain, however, the time-step varies from one iteration to the next as the flow field change. The explicit time-step is the minimum satisfied Courant condition at all points and the Courant number is obligated to be strictly less than 1.

$$\Delta t = \underbrace{\min}_{\forall x}\left(\frac{\mathrm{CFL}\,V(x)}{\lambda_{\max}(x)}, \frac{VNN\,\Delta x^2(x)}{\nu(x)}\right) \tag{2.8}$$

2.3.3.1 The Backward Differentiation Formula Solver

Simcenter STAR-CCM+ uses backward differentiation formulas (BDF) as their time-dependent solver for unsteady implicit problems. BDF can vary from orders one to five, with an increased accuracy with a higher order [10]. This can be explained by expanding Taylor series.

The Taylor expansion series is shown in (2.9). In this equation, h represents the spatial step-size and defined as $h = x_{i+1} - x_i$ [10].

$$f(x_{i+1}) = f(x_i) + f'(x_i)\,h + \frac{f''(x_i)}{2!}h^2 + \frac{f^{(3)}(x_i)}{3!}h^3 + \cdots + \frac{f^n(x_i)}{n!}h^n + R_n \quad (2.9)$$

R_n in (2.10) is the reminder term also called truncation error [10].

$$R_n = \frac{f^{(n+1)}(\xi)}{(n+1)!}h^{n+1} \quad (2.10)$$

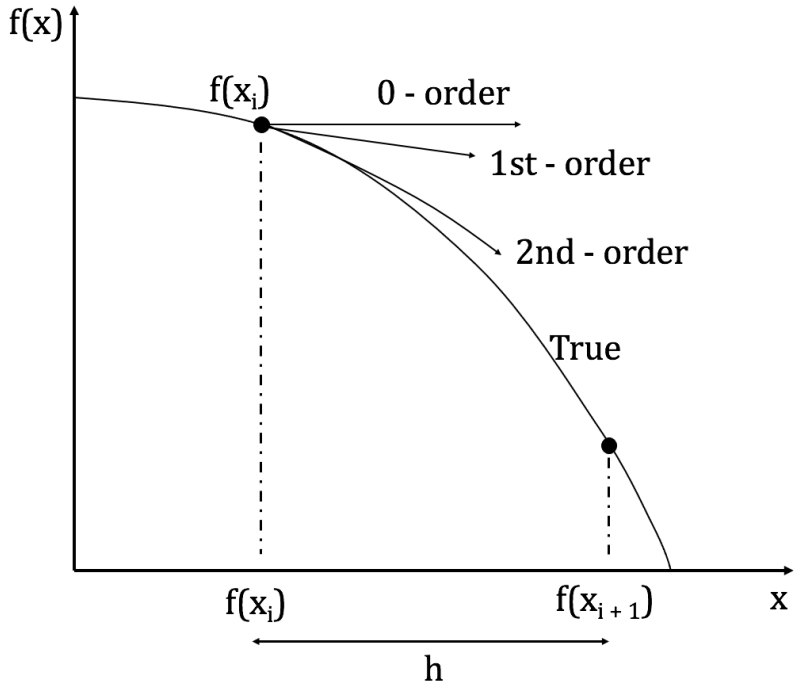

Figure 2.2: Taylor expansion series [10]

The total numerical error is the sum of truncation error and round-off error. Round-off error when a number of decimals are rounded-off in each solution. Truncation errors arise from when the mathematical equations are approximated in the numerical solver. A iterative solution will always have a error where the size of the truncation error are proportional to the order of time step-size.

The truncation error can be reduced by using a smaller step-size whereas the round-off error cannot be changed. The round-off error can however increase if the step-size is too small, due to subtractive cancellation.

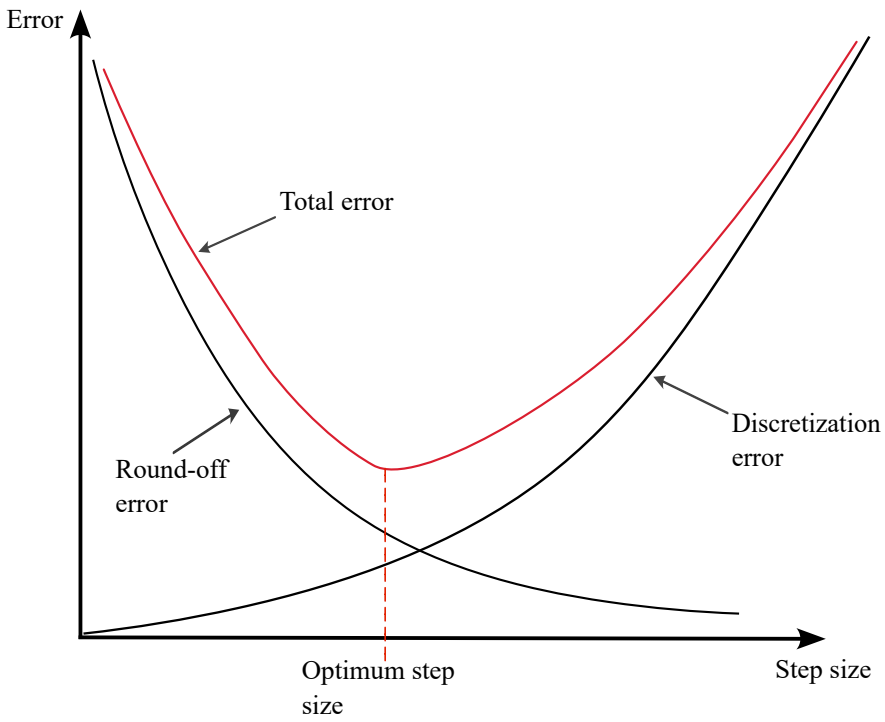

Figure 2.3: Round-off and discretization error [9]

2.3.4 Boundary Conditions

The boundary conditions state the fluid behavior at the boundaries of the domain. Using right boundary conditions are required for both fluid and thermal physics.

2.3.4.1 Wall

- No-slip wall: A boundary condition between fluid and solid. No-slip implies that the fluid boundary layer velocity is equal to the boundary layer velocity.
- Convection wall: A boundary layer condition with a declared heat transfer coefficient used in the governing equations of fluid flow and energy equation.
- Adiabatic wall: This boundary condition state that no flow or heat is transferred across a adiabatic wall.

2.3.4.2 Symmetry Plane

A symmetry plane can be used to reduce the size of the computational domain [2]. The symmetry plane mirrors the domain and all normal gradients and normal velocity are zero on the surface of the boundary. Consequently, there is zero flux across the symmetry plane, and a symmetry plane should only be used when both geometry and flow is symmetric.

$$\vec{u} \cdot \vec{n} = 0, \quad \frac{\partial \vec{u}_{\mathrm{t}}}{\partial n} = 0, \quad \frac{\partial \phi}{\partial n} = 0 \tag{2.11}$$

2.3.5 Mesh

A mesh, also called grid is when the geometric domain is discretized into a set of discrete cell elements. The conservation laws are solved in each cell element, and therefore will a finer mesh improve the numerical accuracy, with the expense of a more computational resource heavy solution. The three dimensional mesh typically consist of a surface mesh, core volume mesh and prism layer mesh.

The surface remesher in STAR-CCM+ consists of triangle shaped cells that define the CAD geometry and prepare for the volume mesh. The polyhedral mesh is a volumetric mesh for 3D simulations. Polyhedral mesh consists of many unstructured faces [2]. Some of the polyhedral meshes advantages is the reduced risk of skewed cells, as well as the reduced number of cells. The many faces of the polyhedral mesh is also advantageous for solving different patterns of flow gradients.

The prism layer mesh create inflation layers at the boundaries of the domain [2]. When the flow variables changes rapidly normal to the boundaries, prism layers improve resolution with a lower number of cells.

2.3.5.1 Mesh Quality

The solver is highly dependent on the quality of the mesh [2]. A mesh of poor quality can result in operational inefficiencies and reliability issues. A mesh with a higher number of skewed cells, or a mesh with a few highly skewed cells can result in convergence issues. Convergence issues can also arise due to rapid changes in cell size or cells with a high aspect ratio. Geometries with sharp corners or small angles always has a high risk of generating cells with high skewness, it is therefore advised to cut and smooth corners of the geometry before generating a mesh.

2.3.5.2 Mesh Independent Study

A mesh sensitivity study or also called mesh independence study show the solver's numerical independence of the solution. There are different approaches to execute the independence study. Typically, a new simulation is conducted with a increased grid resolution [2]. If the solution is significant different compared to the previous solution, another simulation is conducted with a finer grid. This is repeated until no larger changes is seen.

3
Methods

3.1 Experimental Test

The experimental data is gathered from a experimental test called standing heat-loss test, executed according to SIS standard [11]. The water inside the tank was heated to a fixed temperature, and when a uniform temperature had been achieved the tank was left to cool down. As the tank cooled down the temperature was monitored every 10 seconds of the uninsulated tank and every 60 minutes of the insulated tank. As shown in figure 3.1, four sensors were monitoring the temperature inside the tank and four sensors on the outside of the tank. To capture the thermal stratification, the sensors were placed on different tank heights. Two sensors were also placed inside the room to measure the room temperature.

The sensors used for monitoring temperatures had an error of 0.5 °C. The tank is a vertical cylinder, the vessel of the tank is of stainless steel and the heat insulation material is of polyurethane (PUR).

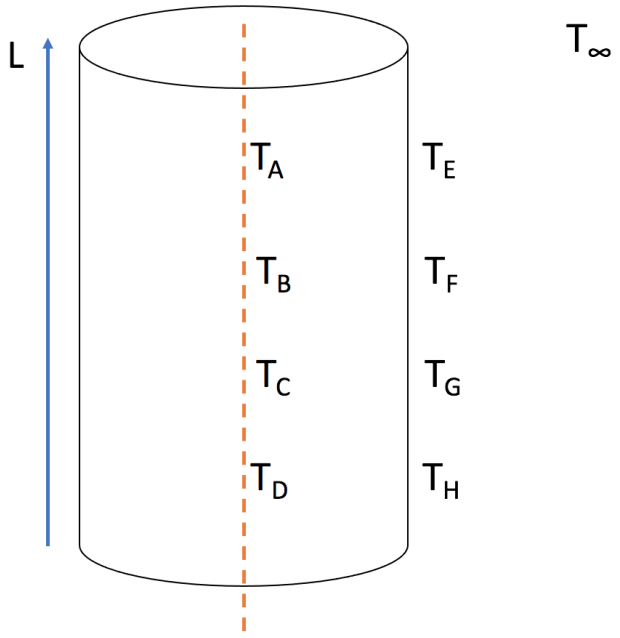

Figure 3.1: Vertical cylinder with temperature sensors placed on different heights

3.2 Initial Calculations

Before the simulation setup, a few analytical one-dimensional steady state calculations were performed to obtain an overview of how different parameters of heat transfer impact the results. The initial calculations were carried out on a vertical cylinder with the assumption that the curvature is small enough to approximate it as a vertical plate. Other assumptions had to be made as well since the experimental test lacked sensors measuring the temperature on the inside of the stainless steel wall as well as outside on the insulated surface in the insulated tank case. Precise values of the material properties such as thermal conductivity and thermal emissivity were also unknown and estimated values were extracted from other material data bases. The real insulated tank had a square shaped insulation surrounding the vertical cylinder tank, and hence the insulation thickness is discontinuous. In the analytical calculations, the thickness was however assumed to be an added layer of material outside of the stainless steel solid.

Figure 3.2 shows a schematic figure of a vertical cylinder with thermal resistances. T_1 is the water temperature at the start of the experimental test, T_{1s} is the assumed inner wall temperature, T_{2s} is the outer wall temperature and T_∞ is the ambient air temperature. k is the thermal conductivity, and r_1 and r_2 are the inner and outer radius of the solid. Heat loss Q was calculated with a total resistance R_{tot}. The equations for thermal resistance are found in Appendix A.

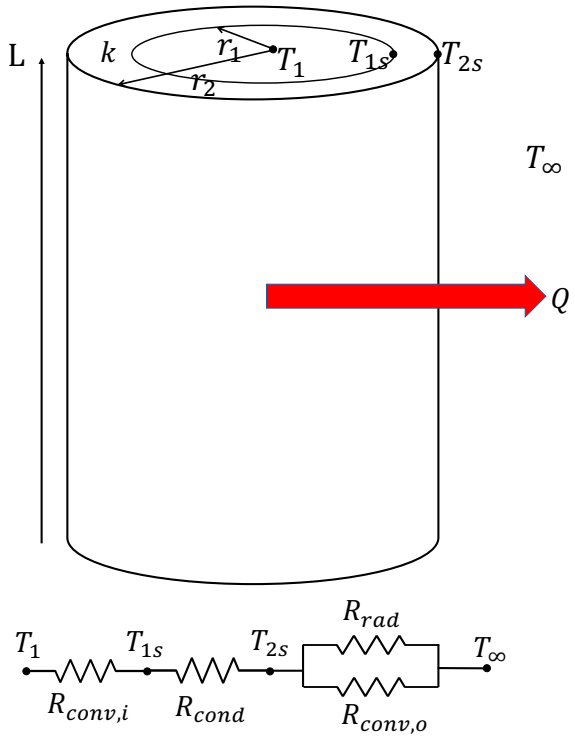

Figure 3.2: Thermal resistance

3.2.1 Sensitivity of Initial Calculations

Each heat transfer method from the inside of the tank to the outside of the tank were approximated as a thermal resistance and combined as a total thermal resistance R_{tot}. Each resistance R_{conv}, R_{cond} and R_{rad} were calculated individually with temperatures measured at the start of the experimental test. The resistances in series R_{conv_i} and R_{cond} were then added together with a parallel resistance of R_{rad} R_{conv_o}. This total resistance R_{tot} was used to calculate heat transfer Q. The hot water T_1 and ambient air T_{amb} was used for ΔT.

This calculated heat transfer value is called Q_{before} in the sensitivity study of resistances. One thermal resistance at a time was multiplied with a factor of 2, and as well as divided with 2, with all other resistances unchanged. This new resistance R_{after} was used in the calculation of a new R_{tot}, and this new R_{tot} was used to calculate a new value of heat transfer Q called Q_{after}. Q_{before} and Q_{after} was then used to calculate the percentage change in heat transfer. This was done one at a time for all resistances.

The Rayleigh number as well as the heat transfer coefficient of convection h_{conv} depends on the characteristic length L i.e. the tank height. Calculations with a L of 0.9, 0.7, 0.5, 0.3, 0.1 meters were carried out to see how h_{conv} and Q were impacted by different tank heights. R_{rad} was also calculated at each height to be able to compare its impact on total heat loss. A new R_{tot} and Q was calculated at each height.

Additional calculations were also carried out where each method of heat transfer were approximated as a heat transfer coefficient h and added together as a overall heat transfer coefficient U. The results of these calculations are found in Appendix B.

3.3 Geometry

ANSA is a tool specifically used for pre-processing [12]. ANSA can be used for all pre-processing stages, however, in this problem ANSA was only used as a CAD clean-up tool to prepare the geometry for mesh and boundary settings in STAR-CCM+.

The work of CAD-cleanup include removing overlapping parts, to smooth surfaces and close gaps. This is done to improve the workflow of the later stages of the CFD process. If the CAD cleaning is performed badly, problems with meshing as well as convergence issues can occur. A well cleaned CAD will also result in more efficient file that require less CPU and memory. The mesh quality decreases if the geometry consists of sharp corners and other small angles. The provided CAD for the uninsulated tank had details such as screws, gasket and a bracket that caused poorly shaped cells and consequently decrease the mesh quality. These details were assumed to have insignificant contribution to the simulated results and they were therefore removed to achieve an improved mesh quality and a simpler geometry. The uninsulated tank after CAD-cleaning is shown in figure 3.3b. The geometry was checked for gaps and other geometric issues before it was saved and imported to STAR-CCM+.

Figure 3.3a shows the insulated tank geometry. This geometry was not used due to a large amount of details resulting in a poor-quality mesh. It also requires a large amount of cells that increase computation time. The uninsulated tank geometry shown in figure 3.3b was used for both the insulated and uninsulated tank simulations.

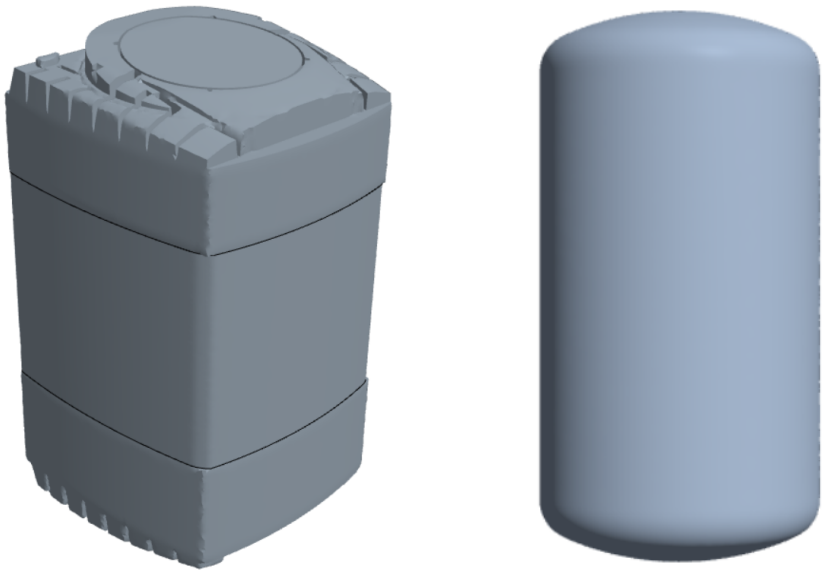

(a) Insulated tank **(b)** Uninsulated tank

Figure 3.3: Geometries of insulated and uninsulated tank

3.4 CFD Process

Simulations of both the uninsulated and insulated tank had been performed before at NIBE. The results were unsuccessful and the numerical setup was therefore reworked with a particular focus on improving the numerical results. The results from the previous setup was used as a benchmark to verify that the simplifications in the reworked version did not alter the results.

Figure 3.4 is a visual presentation of the numerical method. The geometry is first cleaned and meshed, material properties are set, settings for solver and boundary conditions as well as the solution. The results after running a simulation was compared to experimental data and if the correlation is weak, a new process was setup and new runs was iterated until satisfied correlation.

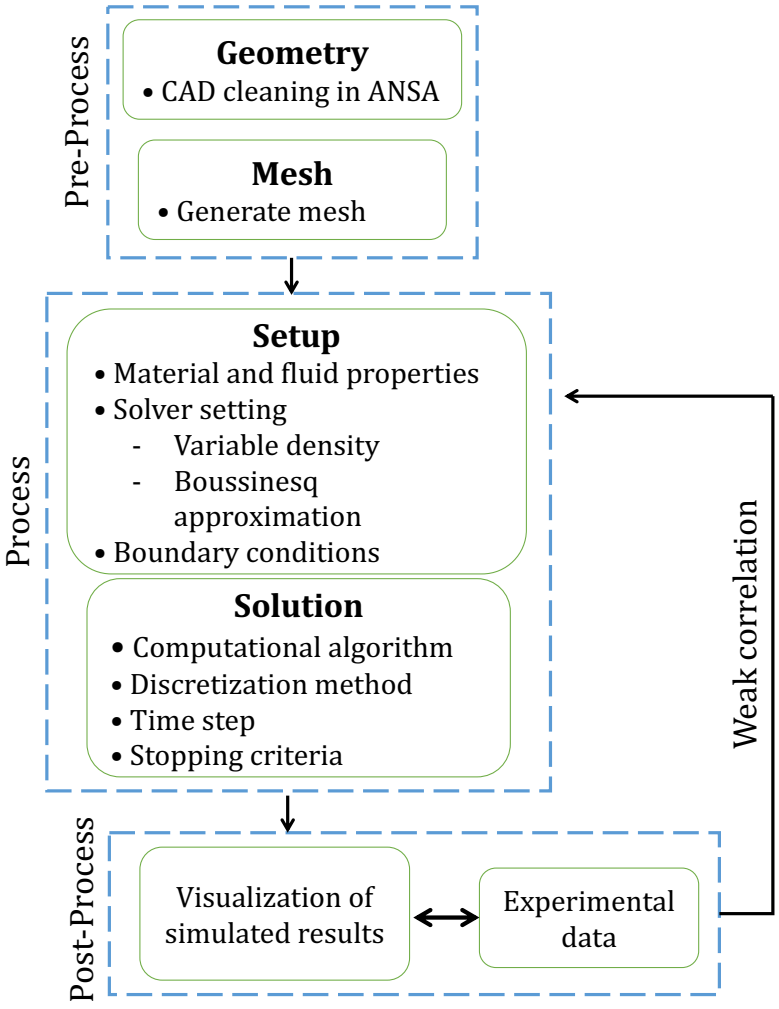

Figure 3.4: Numerical method [13]

As in the experimental setup four monitors were placed on the same tank heights in the middle of the tank and four on the outside of the tank wall. The reworked numerical setup included a change in boundary condition, solver setting, and time-marching approach. From the literature analysis, the flow was assumed to be laminar and the numerical approach was initially solved with a fully coupled approach.

A table including the options of governing equations as well as boundary condition of both uninsulated and insulated model is shown in table 3.1. Constant h stands for a using a single heat transfer coefficient value on the convective boundary condition. Height h stands for a convective boundary condition with different heat transfer coefficients on different heights of the tank and Constant h + Height h is the combined heat transfer coefficient of convective heat transfer coefficient and radiation. The table included a numerical setup of either the polynomial density used for problems with larger temperature differences and the Boussinesq approximation for problems with smaller temperature differences. A decision tree was then used to decide in which order to try out the modeling options.

Table 3.1: Options of different setups

SIM ID	Governing equations	$h\,[W/m^2K]$
P1	Polynomial density	Constant
P2	Polynomial density	Height
P3	Polynomial density	Constant + Rad
P4	Polynomial density	Height + Rad
B1	Boussinesq approximation	Constant
B2	Boussinesq approximation	Height
B3	Boussinesq approximation	Constant + Rad
B4	Boussinesq approximation	Height + Rad

3.4.1 Uninsulated Tank

The geometry was split two times to reduce the domain and thus cell count. Simulating on 1/4 of the geometry decreases computational time and memory. The z-axis was aligned in the center of the tank, one symmetry plane was aligned in the $x = 0$ and the other in $y = 0$. The geometry is shown from the side and top in figure 3.5. The pink color is the fluid region and the gray solid region. To validate that a 1/4 domain did not change the simulated results a comparison of the simulated results between the whole domain and 1/4 domain was carried out. The comparison showed no numerical changes between the simulations and thus all further simulations made was with the 1/4 geometry.

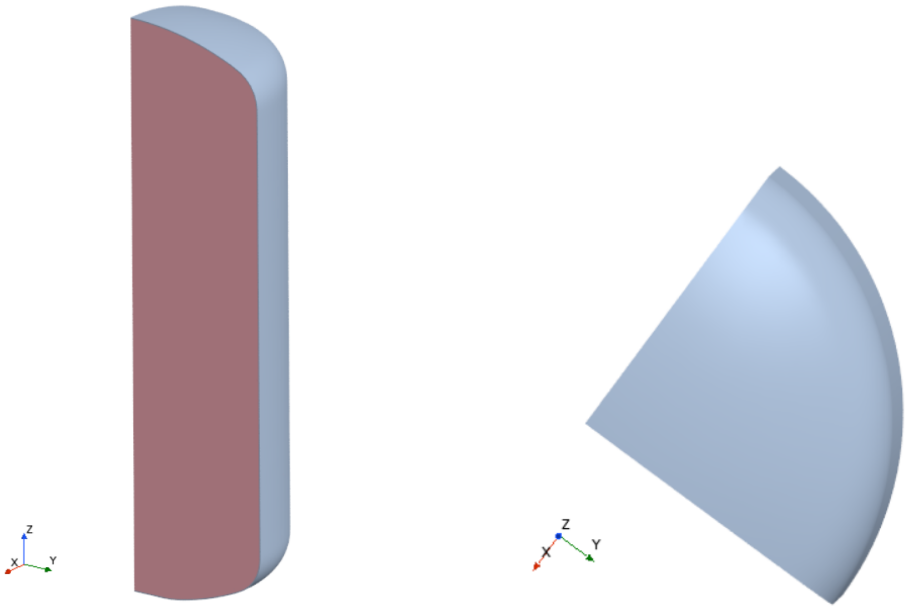

(a) Side view of 1/4 geometry **(b)** Top view of 1/4 geometry

Figure 3.5: 1/4 geometry

Next comparison was between a setup using the Boussinesq approximation and the polynomial density. The numerical results showed no change between the simulations and since the Boussinseq model is less computer heavy, all further simulations carried out was with 1/4 geometry and the Boussinesq model.

To improve correlation between numerical results and experimental data the focus was to change the heat transfer coefficient value on the convection boundary condition. The original model used a constant heat transfer coefficient of 5 W/m^2K. A constant heat transfer coefficient of 4.2 W/m^2K was carried out before using a approach of different heat transfer coefficients on different tank heights.

Figure 3.6 shows the decision tree of in which order to carry out the setups of the uninsulated tank. A comparison was first carried out between using a variable density approach with polynomial density to the Boussinesq approximation. After that, two simulations were carried out between using a constant heat transfer coefficient Const h, to different heat transfer coefficients based on tank height Height h. If correlation to experimental data still is not satisfied, next is to also include radiation in the simulation.

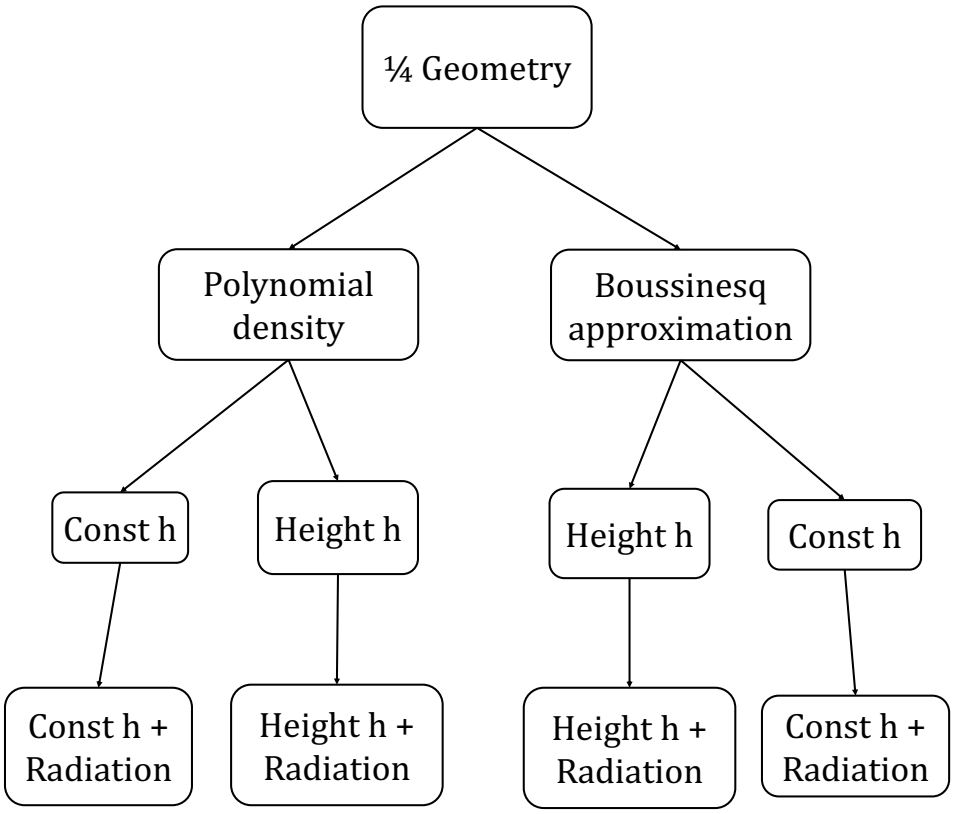

Figure 3.6: Decision tree, uninsulated tank

3.4.1.1 Simulation Setup

Table 3.2 shows the final numerical setup of fluid and solid continua. The Boussinesq model was selected after constant density and gravity had been selected. Implicit unsteady and the fully coupled solver was chosen because of its stability and recommendation for buoyancy driven flow, and with zero initial flow, the fluid was assumed to be laminar. Solution interpolation provide the function of mapping all of the solution data to the next mesh. The reference values for gravity term was assumed to be 9.81 m/s^2 and the atmospheric pressure was set to 101325 Pa.

The initial conditions of water included a fixed static temperature T, and a initial velocity u as zero in every position. Density, dynamic viscosity, specific heat, thermal conductivity and thermal expansion coefficient was added accordingly to the water temperature.

The stainless steel was assumed to have a density ρ of 7850 kg/m^3, specific heat C_p of 480 J/kgK and a thermal conductivity κ of 23 W/mK.

Table 3.2: Continua of uninsulated tank

Continua	**Physics Setup**
Fluid: Water	Boussinesq model Constant density Coupled Energy Coupled Flow Gradients Gravity Implicit Unsteady Laminar Liquid Solution Interpolation Three Dimensional
Solid: Stainless Steel	Constant Density Coupled Solid Energy Gradients Implicit Unsteady Solid Solution Interpolation Three Dimensional

3.4.2 Insulated Tank

Similar as in the case of the uninsulated tank, previous simulations on the insulated tank showed unrealistic results. Which parameter causing the unrealistic results was unknown.

The tank geometry with insulation had many details which caused irregular and deformed cells. Each detail also required a different boundary condition, and the number of cells increased considerably with the added insulation. The choice was therefore to use the same geometry as before and change continua and boundary conditions. An additional positive aspect with this choice was that no time had to be spent on CAD-cleaning.

Figure 3.7 shows the decision tree of the insulated tank. The polynomial density was removed as an alternative since the Boussinesq model had been established to work in the previous uninsulated tank simulations.

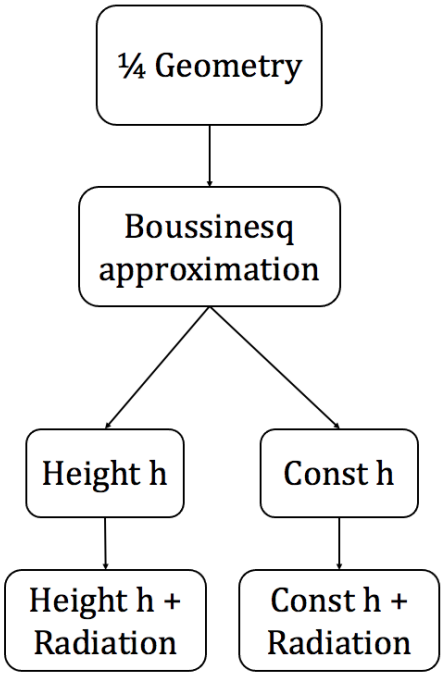

Figure 3.7: Decision tree, insulated tank

3.4.2.1 Simulation Setup

To include material properties of the insulation material PUR, the solid was selected as multi-component solid. This choice made it possible to add properties of both stainless steel and PUR.

The density of polyurethane was assumed to be 25 kg/m^3, the thermal conductivity 0.025 W/mK and the specific heat was assumed to be 0. The material properties of stainless steel was unchanged from previous simulation.

Table 3.3: Continua of insulated tank

Continua	**Physics setup**
Fluid: Water	Boussinesq model Constant density Coupled Energy Coupled Flow Gradients Gravity Implicit Unsteady Laminar Liquid Solution Interpolation Three Dimensional
Solid: Stainless Steel + PUR	Constant Density Gradients Implicit Unsteady Multi-Component Solid Multi-Part Solid Segregated Solid Energy Solution Interpolation Three Dimensional

3.5 Sensitivity Study

When the results from the simulations were correlated to the experimental data, a sensitivity study of the mesh and time-marching was carried out. A mesh study is important for achieving independent numerical results and the time-step study was performed with the purpose of minimizing the computational time.

3.5.1 Mesh Study

The wall on the inside of the tank has the largest changes in fluid movement. When a mesh diagnostics was run on the original mesh the skewness angle was often over 85%, which is a mesh of poor quality. The main focus was therefore to improve the resolution at the boundaries and decrease the skewness angle. Since the computer resources was limited, the mesh study was carried out with an additional two different setups of mesh. The details of mesh setups are seen in 3.4.

The mesh study was carried out with a time-step size of 1 s with the 2-nd order temporal scheme.

Table 3.4: Mesh study setup

Mesh	**Original Mesh**	**Fine Mesh**	**Finer Mesh**
Base Size [m]	0.05	0.04	0.04
Target Surface Size [m]	0.05	0.02	0.02
Minimum Surface Size [m]	0.01	0.01	0.005
Thin Layers [n]	4	4	6
Prism Layer [n]	3	9	18
Cell count [n]	32186	52365	105039

3.5.2 Time-Step Study

Selecting a new time-step size that did not alter the results began by running the simulation locally on the computer with a few cores and changing settings on the fly. While different time-step settings were changed, quantities such as temperature, temperature gradient and the simulation residuals were observed visually to see how the system responded.

The implicit approach uses a pseudo time-step where each time-step are iterated a number of times to converge each time-step solution. Not enough iterations will push the right solution forward and transform the results and too many iterations will increase computation time and resources. To reduce the computation time, it was therefore decried to have the largest time-step size with the lowest number of inner iterations (pseudo time-step) for each time-step.

The time-step study included a comparison of different time-marching approaches such as a fixed time-step, a multi time-step approach, as well as a minimum convergence stopping criteria. The time-step study also included a comparison between how the system responded to a implicit temporal scheme of 1st-order versus 2nd-order. A selected number of tested time-marching cases are found in table 3.5.

Table 3.5: Time-marching study

Case 1	**Case 2**	**Case 3**	**Case 4**
1st-order	1st-order	2nd-order	2nd-order
Step: 0.5 s	Step: 2 s	Step: 4 s	Step: 1 s
Inner Iter: 15	Inner Iter: 25	Inner Iter: 15	Conv Crit: 10^{-4}
Case 5	**Case 6**	**Case 7**	**Case 8**
2nd-order	2nd-order	1st-order	2nd-order
Step: 4 s	4 s $<$ Step $<$ 15 s	Step: 5 s	4 s $<$ Step $<$ 50 s
Conv Crit: 10^{-6}	Inner Iter: 15–35	Inner Iter: 50	Inner Iter: 15-50

4

Results and Discussion

4.1 Initial calculations

The sensitivity of each assumed material property was tried out though a sensitivity analysis where each method of heat transfer were approximated as a thermal resistance and multiplied and divided by 2. The results are seen in table 4.1, where the first column shows the resistance R with the calculated analytical value and the fifth column the sensitivity to a change in the analytical value relatively to total heat loss Q.

Stainless steel on the second row has the lowest thermal resistance and a change in its material property has negligible contributing factor to the total heat loss. Heat transfer through convection from the surrounding air on the third row has the most sensitivity to the assumed value and thermal radiation on the fourth row is secondly most sensitive to its assumed value. If the correlation between experimental and numerical results is weak, a change in the assumed heat transfer coefficient or assumed emissivity of stainless steel will have the most substantial change of the numerical results.

Table 4.1: Sensitivity of the calculated analytical thermal resistance, uninsulated tank

R_{before}	R_{new}	Q_{before}	Q_{after}	% *change*
0.007	R_{conv_i} / 2	98.70	100.20	1.51
	$R_{conv_i} \times 2$	98.70	95.85	2.89
0.0007	R_{steel} / 2	98.70	98.85	0.15
	$R_{steel} \times 2$	98.70	98.42	0.30
0.3	R_{conv_o} / 2	98.70	168.71	70.92
	$R_{conv_o} \times 2$	98.70	62.40	36.78
0.9	R_{rad} / 2	98.70	122.28	23.88
	$R_{rad} \times 2$	98.70	86.78	12.09

Table 4.2 shows the sensitivity analysis results of the insulated tank. The heat insulating material PUR on the third row has the highest thermal resistance and the largest sensitivity to its assumed value. A change in the material property will have the largest change of the numerical results.

Table 4.2: Sensitivity of the calculated analytical thermal resistance, insulated tank

R_{before}	R_{new}	Q_{before}	Q_{after}	% *change*
0.0065	R_{conv_i} / 2	15.04	15.06	0.21
	$R_{conv_i} \times 2$	15.04	14.97	0.43
0.00063	R_{steel} / 2	15.04	15.03	0.02
	$R_{steel} \times 2$	15.04	15.02	0.04
1.36	R_{PUR} / 2	15.04	27.01	44.37
	$R_{PUR} \times 2$	15.04	7.96	88.73
0.64	R_{conv_o} / 2	15.04	168.71	2.22
	$R_{conv_o} \times 2$	15.04	15.37	2.22
0.22	R_{rad} / 2	15.04	15.76	4.60
	$R_{rad} \times 2$	15.04	14.13	6.37

As heat is lost from the tank to the surrounding air, the air close to the tank heats up and flows up along the tank surface, creating a boundary layer between warmer tank temperature and cooler ambient air. The analytical calculations based on various tank heights are shown in table 4.3. R_{tot} is the total thermal resistance, calculated from the inside of the tank to the outside. An increase in tank height increases thermal resistance R_{tot} and this suggests that the main heat loss occur in the lower tank region which is also seen in column Q_{tot}. R_{conv_o} is the resistance by air on the tank. The air flow increases with tank height and turns from laminar to turbulent natural convection.

Table 4.3: Heat loss, uninsulated tank based on the characteristic length

L	*Air Flow*	R_{conv_o}	R_{rad}	R_{tot}	Q_{tot}
0.9	Turbulent	0.30	0.91	0.23	98.71
0.7	Turbulent	0.30	0.91	0.23	98.71
0.5	Laminar	0.28	0.91	0.22	102.62
0.3	Laminar	0.25	0.91	0.20	112.86
0.1	Laminar	0.19	0.91	0.16	139.52

Heat is mainly lost from the lower tank regions. This is a result of buoyancy and circulating air. Heat loss through thermal radiation is expected to have a larger contributing factor in the higher tank regions as the experimental test and simulation progress. The density differences between warmer and colder fluid will result in a temperature layering, the higher up in the tank the higher temperature. However, the small temperature difference between higher and lower tank regions is most likely to have a limited impact.

As the water temperature decreases the driving force of convective heat loss will decrease and it is possible that thermal radiation will have a larger contributing factor in the end of the transient simulation. The analytical calculations are solely based on temperatures at the start of the experimental test when the water is the warmest. The time dependent heat loss is therefore not visible in the presented analytical calculations.

The analytical calculations based on various tank heights of the insulated tank are shown in table 4.4. The air flow is laminar in every tank height. Even though the convective resistance is different on different tank heights, the total heat loss Q_{tot} in the fifth column varies very little. The reason for this is in all likelihood the larger resistance of the insulating material.

Table 4.4: Heat loss, insulated tank based on the characteristic length

L	*Air Flow*	R_{conv_o}	R_{rad}	R_{tot}	Q_{tot}
0.9	Laminar	0.66	0.22	1.53	15.02
0.7	Laminar	0.62	0.22	1.53	15.04
0.5	Laminar	0.57	0.22	1.52	15.08
0.3	Laminar	0.50	0.22	1.52	15.14
0.1	Laminar	0.38	0.22	1.51	15.28

Another difference between the uninsulated and insulated tank is the amount of heat loss through thermal radiation. The resistance of radiation R_{rad} in the third column in figure 4.4 is always lower than the convective resistance of air R_{conv}. This result is opposite compared to the uninsulated tank in figure 4.3 where radiation has higher resistance. The analytical calculations show that heat loss through radiation has a more significant impact on total heat loss when the tank has insulated surfaces. The insulation was of dark color and the emissivity has thus a larger value. Adding a reflective coating with a lower emissivity on top of the dark insulation can lower the heat loss from thermal radiation.

4.2 Simulation Results

All figures with simulated results show the numerical results from the simulations in blue and the experimental data in yellow. The horizontal axis is the physical time and the vertical axis temperature. The water temperature is measured on four different tank heights, TA, TB, TC and TD. The first section shows the numerical results for the uninsulated tank and the second section shows the numerical results for the insulated tank.

4.2.1 Uninsulated Tank

The numerical results of the uninsulated tank include figures of:

1. Constant heat transfer coefficient
2. Constant heat transfer coefficient plus radiation
3. Different heat transfer coefficient for different heights of the tank
4. A comparison between the whole physical domain to the 1/4 domain size

4.2.1.1 Constant Heat Transfer Coefficient

Figure 4.1 shows the numerical results of a constant convective heat transfer coefficient h of 5 W/m^{2}K. The temperature in point, TA, TB, TC, drop too fast and this suggest that a h of 5 W/m^{2}K is too high. However, point TD which measures the temperature in the lower tank region drop too slow compared to experimental data and the h should hence be higher in the lower tank region. The results of a constant h of 4.3 W/m^{2}K is found in Appendix C.

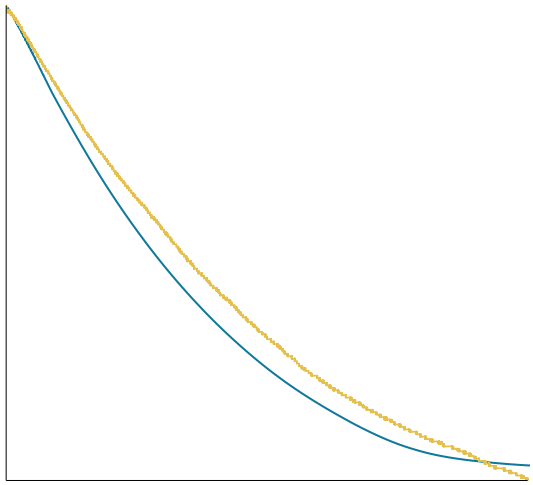

(a) Point TA
High Tank Region

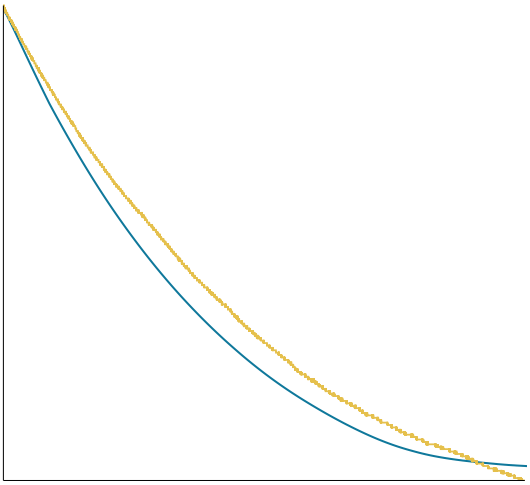

(b) Point TB
Middle Tank Region

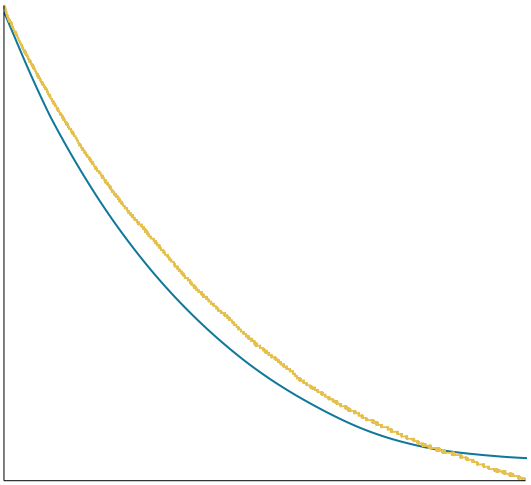

(c) Point TC
Middle Tank Region

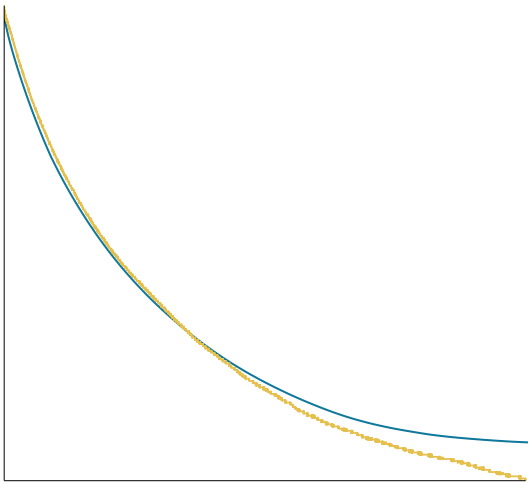

(d) Point TD
Low Tank Region

Figure 4.1: $h_{\text{conv}} = 5\ \text{W}/(\text{m}^2{\cdot}\text{K})$

4.2.1.2 Constant Heat Transfer Coefficient + Radiation

The numerical results of adding radiation to a constant h of 3.5 W/m^{2}K is shown in figure 4.2. The only measuring point to follow the experimental curve is TD, the rest of the sensors drop too quickly and a lower h is required in the higher tank regions.

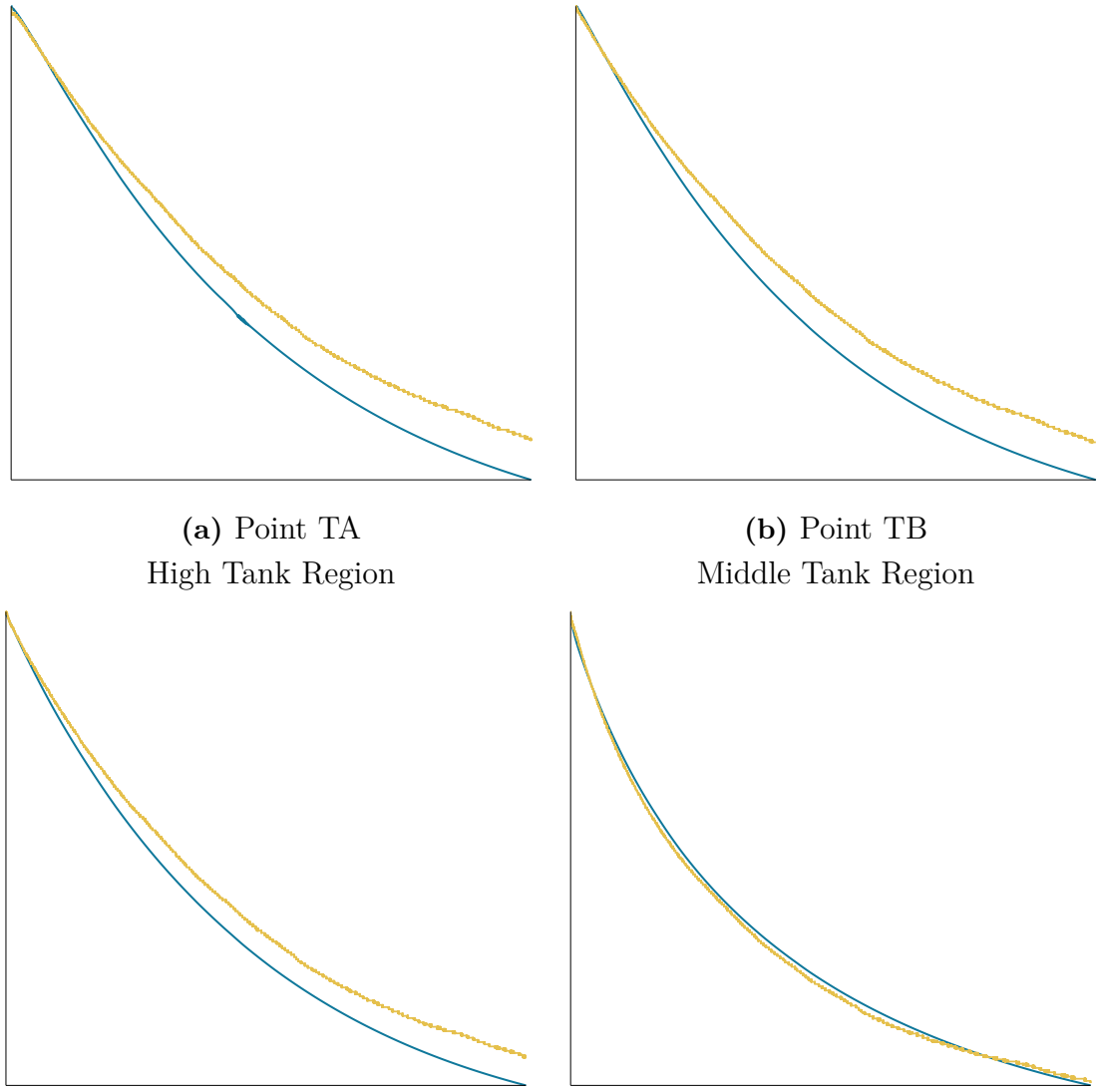

(a) Point TA
High Tank Region

(b) Point TB
Middle Tank Region

(c) Point TC
Middle Tank Region

(d) Point TD
Low Tank Region

Figure 4.2: $h_{\text{conv}} = 3.5$ W/(m^2·K), and $h_{\text{rad}} = 1.0$ W/(m^2·K)

4.2.1.3 Different Heat Transfer Coefficient

The correlation between numerical and experimental results improved with the approach to use different heat transfer coefficients on different heights of the tank, see figure 4.3. A heat transfer coefficient h of approximately 3.5 W/m^{2}K was used on points TA, TB, TC, and a higher value of 5.5 W/m^{2}K was used for point TD. There is a small deviation between numerical and experimental data in the end of the simulations of points TA, TB, TC. A higher h caused the temperatures to drop below the experimental line and therefore, an alternative to improve correlation is to carry out additional simulations where radiation is also included. Also, a change of heat transfer coefficient in point TD with all other unchanged affected the results significantly on all of the points TA, TB, TC and TD.

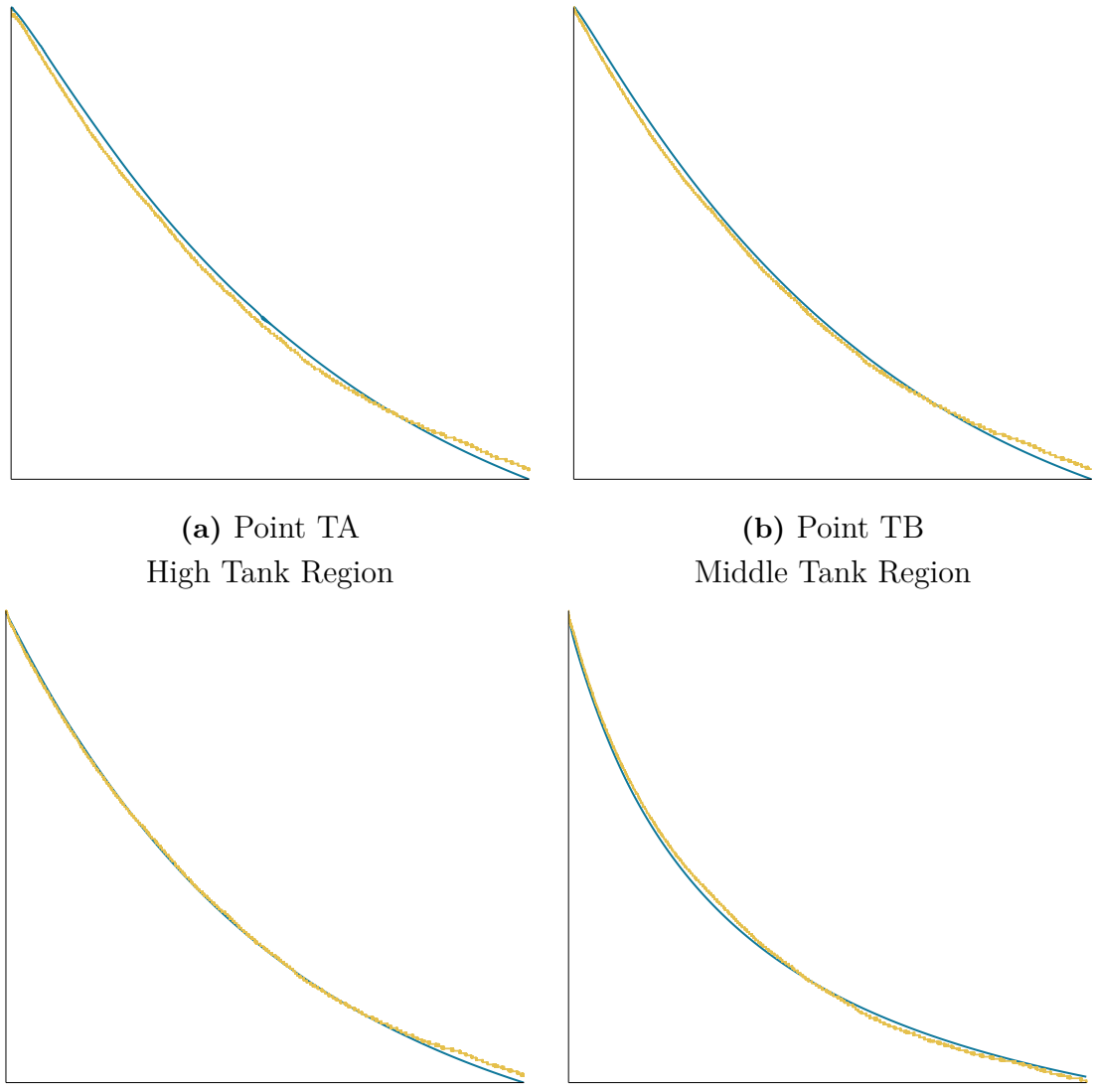

(a) Point TA
High Tank Region

(b) Point TB
Middle Tank Region

(c) Point TC
Middle Tank Region

(d) Point TD
Low Tank Region

Figure 4.3: Different h_{conv} on different heights of 3.5 and 5.5 W/(m^2·K)

4.2.2 Symmetry Plane on Uninsulated Tank

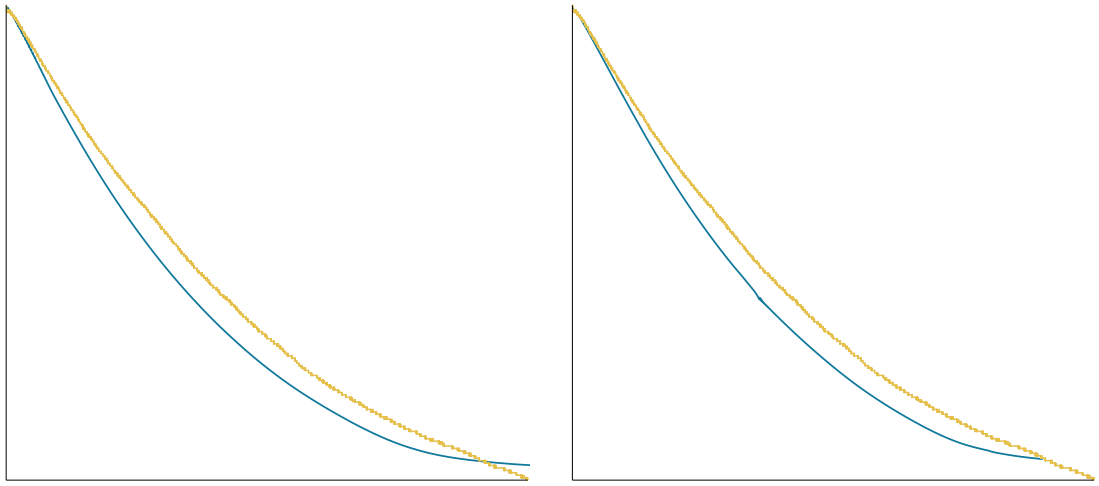

(a) Whole domain **(b)** 1/4 domain

Figure 4.4: Comparison of simulation results between whole domain and 1/4 domain, uninsulated tank

Figure 4.4 shows a comparison of point TA between the numerical results of a whole domain and a reduced domain size. The results show insignificant differences, however, the solver shows to have instability issues approximately in the middle of the blue line on the 1/4 domain in figure 4.4b.

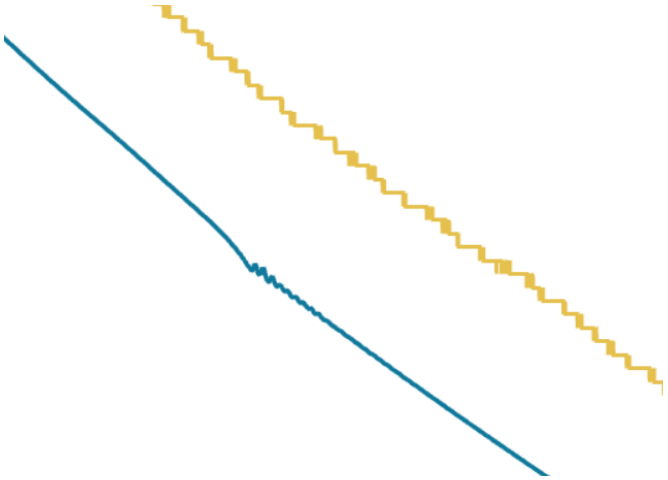

Figure 4.5: Zoom-in on solver instability (blue line) of uninsulated 1/4 tank

A zoom-in of the instability in 4.4b is shown in figure 4.5. Since this instability is solely visible for monitor TA, turbulent fluid flow could be the the reason to this issue. It is possible that a finer mesh could improve capture of fluid pattern and improve solver stability.

The fluid velocity and fluid pattern at the end of the numerical simulation is seen from different perspectives in 4.6. The higher fluid velocities in red as well as turbulent pattern is solely seen in the top regions of the tank.

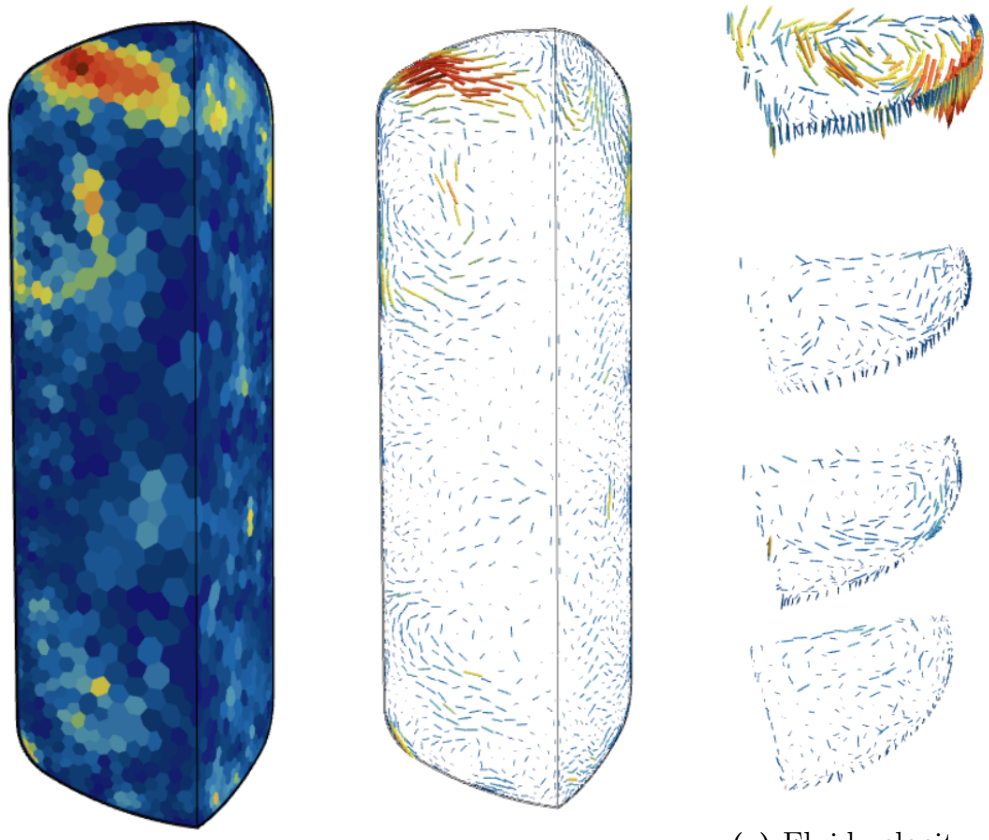

(a) Fluid velocity Scalar view

(b) Fluid velocity Vector field view

(c) Fluid velocity Vector field view 1/4 sections

Figure 4.6: Fluid velocity, uninsulated tank

The red parts have a fluid velocity approximately between 4 to 6 mm/s and the blue parts 0 mm/s. The fluid velocity in vertical z-direction is hence significantly higher compared to x and y-direction. The third figure 4.6c is a vector field of the fluid pattern for each measuring point TA, TB, TC, TD. The turbulent fluid pattern in TA is stronger compared to regions below. The red parts are stronger on one side of the symmetry plane compared to the other. This could indicate that the symmetry planes disrupt fluid flow.

Figure 4.7 shows a larger view of the fluid pattern of plane section TA of the uninsulated tank. The red arrows is the fluid with larger fluid velocity and these red arrows mainly points downwards in the z-direction, along the tank walls.

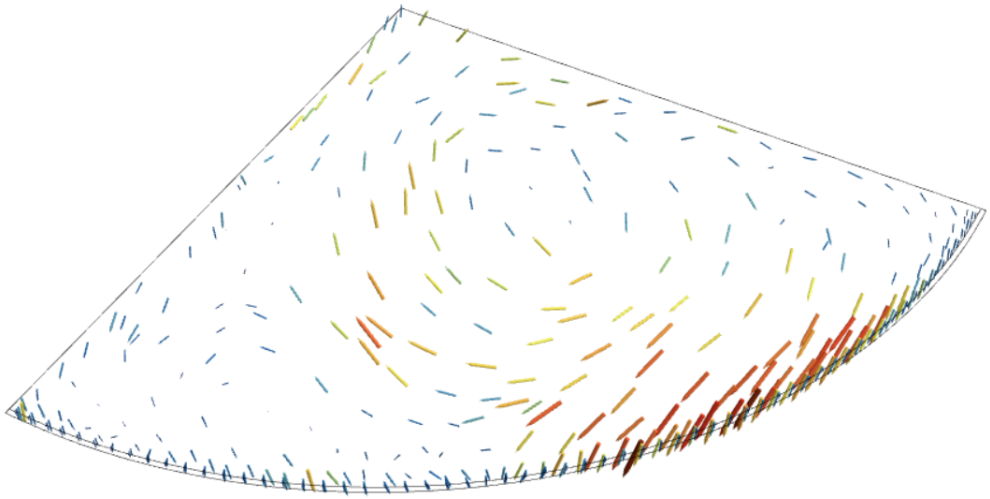

Figure 4.7: 1/4 plane section of TA

4.2.3 Insulated Tank

Insulating the tank surfaces decreases rate of heat loss and as seen in figure 4.8, the experimental data line in yellow is very similar in all of the temperature points and as well linear.

Changing the thickness of the insulation has a large impact on the thermal resistance and as the geometry used for simulations has a thinner solid a parameter that controls heat transfer must be changed to compensate for the lower resistance. A lower h of 1 W/m^{2}K or an increase in thermal resistance made the total heat loss equivalent to a geometry with thicker solid. Figure 4.8 shows the numerical results of point TA, TB, TC, TD when using a h of 1 W/m^{2}K.

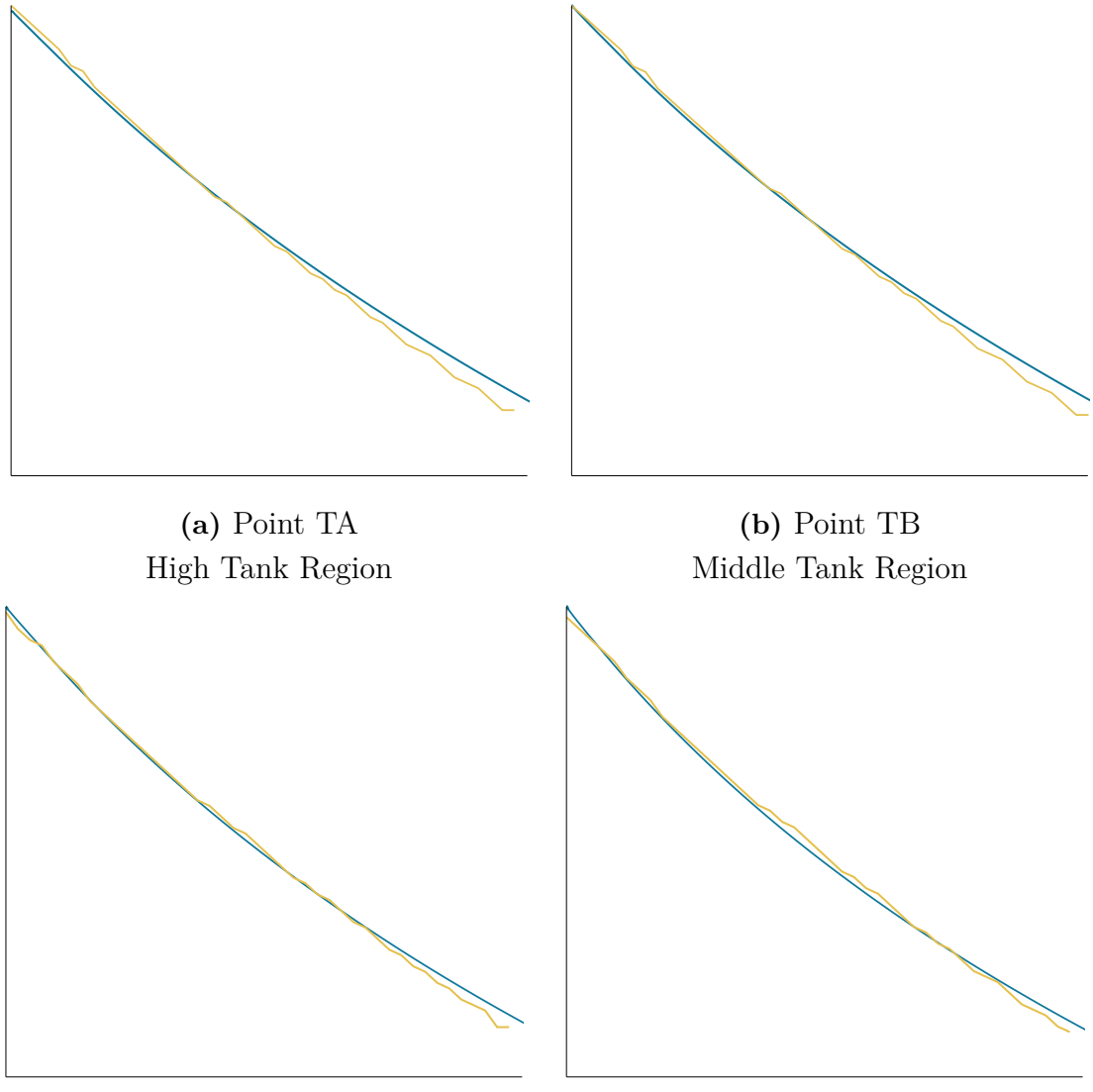

(a) Point TA
High Tank Region

(b) Point TB
Middle Tank Region

(c) Point TC
Middle Tank Region

(d) Point TD
Low Tank Region

Figure 4.8: $h_{\text{conv}} = 1$ W/(m^2·K)

4.2.4 Symmetry Plane on Insulated Tank

Figure 4.9 shows a comparison between the numerical results of the whole domain and 1/4 domain size. No solver instabilities or numerical differences could be seen between simulations on the whole domain and 1/4 of the domain. This can be explained by a reduced rate of heat loss, which in turn make the the fluid flow slower and less turbulent.

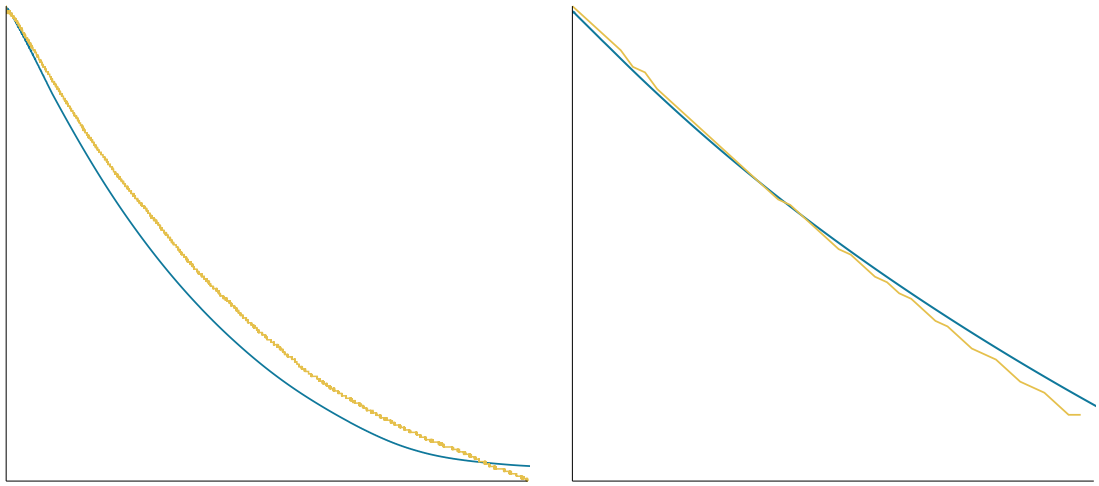

(a) Whole domain **(b)** 1/4 domain

Figure 4.9: Comparison between simulated results of the whole domain and 1/4 domain, insulated tank

The fluid pattern of the insulated tank is identical to the uninsulated tank. A scalar view and vector field view of the insulated tank's fluid pattern can be seen in Figure 4.10. The red parts represents a fluid maximum velocity of 1 to 2 mm/s compared to 6 to 4 mm/s in the uninsulated tank simulations.

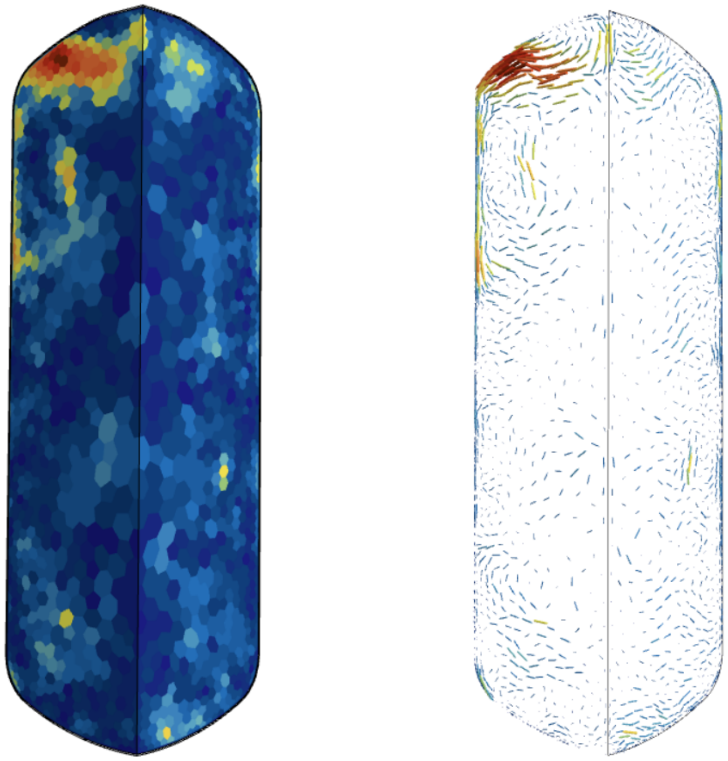

(a) Scalar view of fluid velocity insulated tank

(b) Vector field view of fluid velocity insulated tank

Figure 4.10: Fluid velocity of insulated tank at the end of the experimental test

4.2.5 Mesh Sensitivity Study

It was not possible to perform a well executed mesh sensitivity study due to the limited computational resources. When mesh is refined the number of cells increase, a larger cell count make the simulations heavier. A finer mesh also requires a smaller time-step due to a change in the travel distance of the fluid. This additionally increases the the required computational resources.

4.3 Final Setup

Table 4.5 is a summary of the original and reworked uninsulated tank setup. A constant heat transfer coefficient on the outer tank wall did not correlate with the experimental data. Radiation and a constant heat transfer coefficient did improve the correlation to some degree, however using different heat transfer coefficients on different heights of the tank improved correlation significantly. The 2nd-order implicit scheme made it possible to use a larger time-step and this reduced the overall computation time. However, a higher order of 4 or 5 slowed the solver significantly. A multi-time marching approach combined with a minimum convergence criterion of 10^{-6} had the best reduction of computation time while providing results that correlated to experimental data.

Table 4.5: Original and reworked numerical setup, uninsulated tank

	Original	Reworked
Geometry	1	1/4
Gov. equations	Polynomial density	Boussinesq approx
Conv. BC	Constant: 5	Different, height
Temporal scheme	1st-order	2nd-order
Step size	Constant: 0.5 s	Multiple: 4 s to 25 s
Stop crit	Inner It: 15	Conv crit: 10^{-6} + Min Inner It: 4
Computation time	700 cores, 48 hours	4 cores, 1 hour

Table 4.6 is a summary of the original and reworked insulated tank setup. This simulation required a constant step size as well as a different approach to the pseudo time-step stopping criteria. When a multi time-step approach was used, the numerical results showed nonphysical results since the temperature did not decrease sufficiently when the time-step increased. A large time-step increases the truncation error and with a relatively constant temperature gradient, a constant time-step provided the best accuracy of true physical results. This simulation also required a different stopping criteria. A tight minimum convergence criterion of 10^{-6} was too slow to converge each time-step while a minimum convergence criterion of 10^{-4} did not provide sufficiently converged solutions. The final time marching approach used a convergence criterion of 10^{-5} with an increased number of minimum inner iterations. Increasing the minimum number of inner iterations avoids temporary issues such as constant satisfied convergence criterion. The constant satisfied continuity criterion is most likely also related to a very slow fluid flow.

Table 4.6: Original and reworked numerical setup, insulated tank

	Original	Reworked
Geometry	1/2	1/4
Gov. equations	Polynomial density	Boussinesq approx
Conv. BC	Constant	Constant
Temporal scheme	1st-order	2nd-order
Step size	Constant: 0.5 s	Constant: 4 s
Stop crit	Inner It: 15	Conv crit: 10^{-5} + Min Inner It: 15
Computation time	N/A	4 cores, 2 hours

5
Conclusion

The analytical calculations can be used to understand the physics of thermal behavior but they can not be treated as true or exact values. In this work they gave an initial value of the convection boundary condition. They also gave direction to what is of importance in situations of uncertainty such as correct material data and simplifications. The analytical calculations showed the relevance of different heat transfer coefficients on different heights of the uninsulated tank when the numerical results is to be correlated to an exact local temperature. An air domain can be used instead of a convective boundary condition. This approach is advantageous in situations where exact physical results are desired, or to visualize the air flow on the outside of the tank. The downside is however a larger number of cell elements and hence computation-time.

The 2nd-order implicit scheme made it possible to use a larger time-step and this reduced the overall computation time. However, a higher order of 4 or 5 slowed the solver significantly. A multi-time marching approach combined with a minimum convergence criterion had the best reduction of computation time while providing results that correlated to experimental data. This approach however varies greatly from case to case and larger time-steps approximates solutions and thus this approach is not advised if the goal is to have simulations with numerical independence. The insulated tank required a constant time-step, this is opposite to the uninsulated tank where a multi-time-stepping approach could be used. The reason for this is likely due to the slower rate of heat loss and as well constant temperature gradient.

A common approach to reduce the computation time is to decrease the domain size by using symmetry planes. Symmetry planes can however disrupt fluid flow and alter the numerical results. To remove any uncertainties of a reduced domain size it's advised to do a comparison between the results from the whole domain to the reduced size. This approach can also be used in other cases of uncertainties, such as governing equation approximations of the Navier-Stokes equations.

The simulations with 1/4 of the geometry, the Boussinesq approximation, a multi-time-stepping approach and a minimum convergence criterion reduced the computation time with several hours when all other parameters was unchanged. However, if the solution is to be numerical independent the expected computation time is to be greatly increased. This work included two cases with slow flow velocity, problems with higher fluid flow and turbulence will require a smaller time-step and possible also a stronger stopping criteria.

5.1 Future Work

Future work could include a investigation of:

- Dynamic mode simulations of the tank. This could include discharge and charging of the tank as well as a comparison of fluid flow and thermal stratification with and without a turbulence plate. The turbulence plate act as a barrier decreasing turbulence and mixing. This has shown to improve stratification and efficiency.
- STAR-CCM+ functions. STAR-CCM+ has several functions that make simulations more efficient. For example, stages make it possible to initialize a temperature gradient before starting a transient simulation. This function make it possible to use a larger time-step size from start. The simulation operation loop is a function that can be used to solve fluid and solid separately. This is advantageous in problems dominated by thermal conduction heat transfer since heat travels slower in materials.
- Simulations with a smaller geometry. It was not possible to do greater reductions than 1/4 of the physical geometry for 3D-simulations in STAR-CCM+. The geometry can however first be split in ANSA and then inserted to STAR-CCM+. It is possible that a smaller geometry will transform the simulated results. However, simulations with a smaller geometry will reduce computation time and therefore, smaller deviations between experimental and simulated results be accepted if the gain of computation time is large enough.
- Mesh sensitivity analysis.

Bibliography

[1] J. Tu, G.-H. Yeoh, and C. Liu, "Chapter 1 - introduction," in *Computational Fluid Dynamics (Second Edition)*, J. Tu, G.-H. Yeoh, and C. Liu, Eds., Second Edition, Butterworth-Heinemann, 2013, pp. 1–29, ISBN: 978-0-08-098243-4. DOI: https://doi.org/10.1016/B978-0-08-098243-4.00001-9. [Online]. Available: https://www.sciencedirect.com/science/article/pii/B9780080982434000019.

[2] J. M. C. Yunus A. Çengel, *Fluid Mechanics: Fundamentals and Applications*. New York : McGraw-Hill, 2018.

[3] Siemens Digital Industries Software. "Computational fluid dynamics (cfd) simulation." Accessed: 2025-06-10. (2024), [Online]. Available: https://www.sw.siemens.com/en-US/technology/computational-fluid-dynamics-cfd-simulation/.

[4] Siemens Digital Industries Software. "Mh.5.111 - conjugate heat transfer modeling in star-ccm+." Accessed: 2025-06-01. (2024), [Online]. Available: https://community.sw.siemens.com/s/article/MH-5-111.

[5] J. Lago, F. De Ridder, W. Mazairac, and B. De Schutter, "A 1-dimensional continuous and smooth model for thermally stratified storage tanks including mixing and buoyancy," *Applied Energy*, vol. 248, pp. 640–655, 2019, ISSN: 0306-2619. DOI: https://doi.org/10.1016/j.apenergy.2019.04.139. [Online]. Available: https://www.sciencedirect.com/science/article/pii/S0306261919307901.

[6] D. L. Savicki, H. A. Vielmo, and A. Krenzinger, "Three-dimensional analysis and investigation of the thermal and hydrodynamic behaviors of cylindrical storage tanks," *Renewable Energy*, vol. 36, 2011, ISSN: 0960-1481. DOI: https://doi.org/10.1016/j.renene.2010.10.011. [Online]. Available: https://research.ebsco.com/linkprocessor/plink?id=a870b983-2587-3c90-a563-da7990aeaca4.

[7] F. P. Incropera, D. P. DeWitt, T. L. Bergman, and A. S. Lavine, *Fundamentals of Heat and Mass Transfer*, 6th ed. Hoboken, NJ, USA: John Wiley & Sons, 2006, ISBN: 978-0-471-45728-2.

[8] R. Karwa, *Heat and Mass Transfer*. Springer Singapore, 2017. DOI: https://doi.org/10.1007/978-981-10-1557-1.

[9] A. J. G. Yunus A. Çengel, *Heat and mass transfer : fundamentals and applications*. New York : McGraw-Hill, 2015.

[10] S. C. Chapra and R. P. Canale, *Numerical Methods for Engineers*, 7th ed. New York: McGraw-Hill Education, 2015, ISBN: 978-0-07-339792-4.

[11] Swedish Standards Institute, *Water supply – specification for indirectly heated unvented (closed) storage water heaters*, SS-EN 12897:2016+A1:2020, https://www.sis.se/en/produkter/construction-materials-and-building/installations-in-buildings/water-heating-equipment/ss-en-128972016a1-20202020/, 2020.

[12] B. C. Systems, *A guide to the superiority of beta cae systems software suite*, Brochure, 2021. [Online]. Available: https://www.beta-cae.com/brochure/ansa_meta_superiority.pdf.

[13] M. Wang, E. Hu, and L. Chen, "Cfd analysis and optimization of thermal stratification in a thermal diode tank (tdt)," *Journal of Energy Storage*, vol. 76, p. 109 837, 2024, ISSN: 2352-152X. DOI: 10.1016/j.est.2023.109837. [Online]. Available: https://www.sciencedirect.com/science/article/pii/S2352152X23032358.

A

Appendix 1

Equations of thermal resistance of a vertical cylinder:

$$R_{conv} = \frac{1}{2\pi r L h_{conv}} \tag{A.1}$$

$$R_{cond} = \frac{ln(r_2/r_1)}{2\pi L k} \tag{A.2}$$

$$R_{rad} = \frac{1}{2\pi L h_{rad}} \tag{A.3}$$

$$R_{comb} = \frac{R_{conv}\ R_{rad}}{R_{conv} + R_{rad}} \tag{A.4}$$

$$R_{tot} = R_{conv} + R_{cond} + \frac{R_{conv}\ R_{rad}}{R_{conv} + R_{rad}} \tag{A.5}$$

$$Q = \frac{(T_1 - T_\infty)}{R_{tot}} \tag{A.6}$$

Equations of heat transfer coefficients of a vertical cylinder:

$$h_{cond} = \frac{ln(r_2/r_1)}{k} \tag{A.7}$$

$$h_{rad} = \varepsilon\sigma(T_1 + T_2)(T_1^2 + T_2^2) \tag{A.8}$$

$$h_{comb} = h_{conv} + h_{rad} \tag{A.9}$$

B

Appendix 2

Table B.1: Sensitivity of the calculated analytical heat transfer coefficients, uninsulated tank

h_{before}	h_{new}	Q_{before}	Q_{after}	% *change*
156	h_{conv_i} / 2	98.92	96.25	2.70
	$h_{conv_i} \times 2$	98.92	100.31	1.41
1533	h_{steel} / 2	98.92	98.64	0.28
	$h_{steel} \times 2$	98.92	99.06	0.14
3.35	h_{conv_o} / 2	98.92	62.49	36.83
	$h_{conv_o} \times 2$	98.92	169.34	71.19
1.11	h_{rad} / 2	98.92	86.94	12.11
	$h_{rad} \times 2$	98.92	122.61	23.94

Table B.2: Sensitivity of the calculated analytical heat transfer coefficients, insulated tank

h_{before}	h_{new}	Q_{before}	Q_{after}	% *change*
152.40	h_{conv_i} / 2	17.48	17.41	0.39
	$h_{conv_i} \times 2$	17.48	17.52	0.19
1590	h_{steel} / 2	17.48	17.47	0.04
	$h_{steel} \times 2$	17.48	17.48	0.02
0.68	h_{PUR} / 2	17.48	9.35	46.53
	$h_{PUR} \times 2$	17.48	30.94	77.01
1.22	h_{conv_o} / 2	17.48	17.16	1.83
	$h_{conv_o} \times 2$	17.48	17.94	2.64
3.50	h_{rad} / 2	17.48	16.28	6.90
	$h_{rad} \times 2$	17.48	18.47	5.65

Table B.3: Heat loss uninsulated tank based on the characteristic length

L	h_{conv_o}	h_{rad}	U	Q_{tot}
0.9	3.35	1.11	4.32	98.92
0.7	3.35	1.11	4.32	98.92
0.5	3.53	1.11	4.49	102.85
0.3	4.01	1.11	4.94	113.14
0.1	5.28	1.11	6.11	139.95

Table B.4: Heat loss insulated tank based on the characteristic length

L	h_{conv_o}	h_{rad}	U	Q_{tot}
0.9	1.18	0.22	0.59	17.46
0.7	1.26	0.22	0.59	17.50
0.5	1.37	0.22	0.60	17.55
0.3	1.56	0.22	0.60	17.63
0.1	2.05	0.22	0.60	17.82

C
Appendix 3

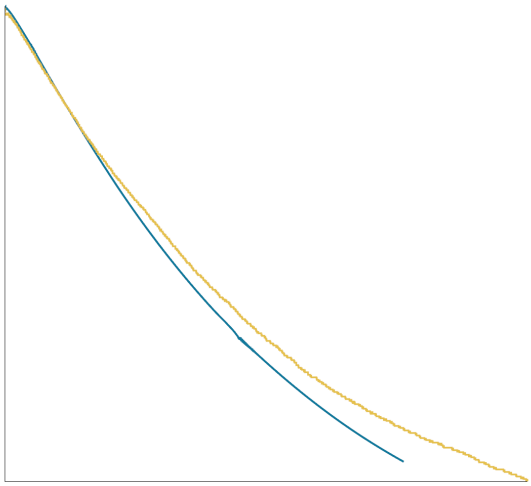

(a) Point TA
High Tank Region

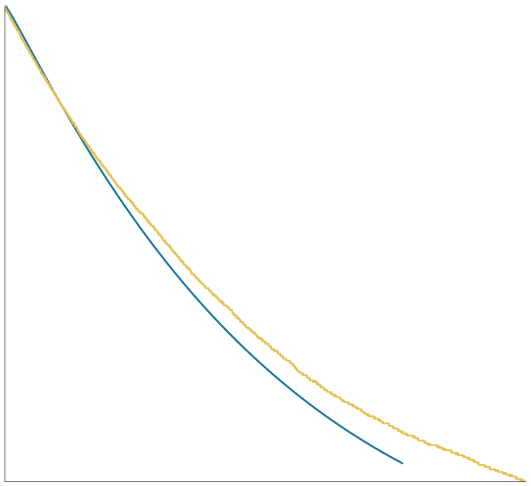

(b) Point TB
Middle Tank Region

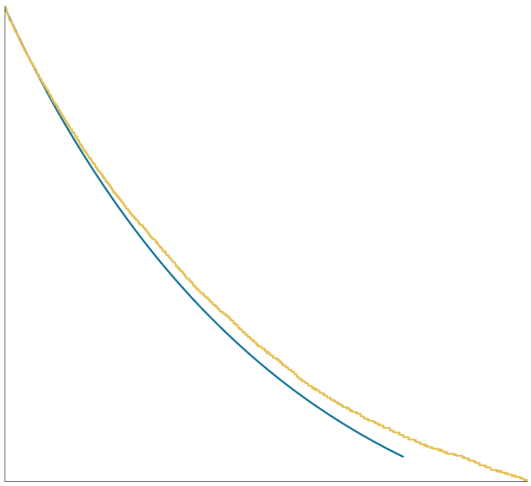

(c) Point TC
Middle Tank Region

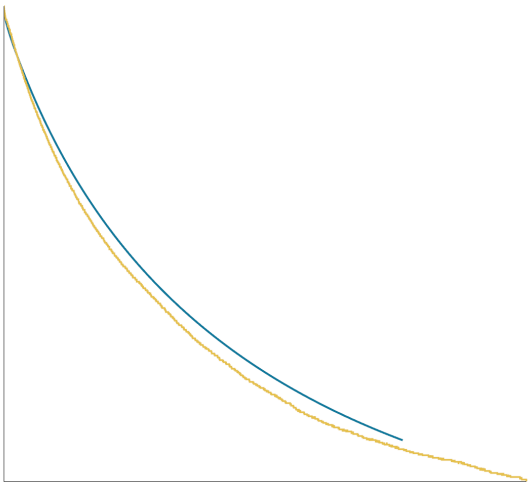

(d) Point TD
Low Tank Region

Figure C.1: $h_{\text{conv}} = 4.3\ \text{W}/(\text{m}^2{\cdot}\text{K})$

DEPARTMENT OF MECHANICS AND MARITIME SCIENCES
CHALMERS UNIVERSITY OF TECHNOLOGY
Gothenburg, Sweden
www.chalmers.se

CHALMERS
UNIVERSITY OF TECHNOLOGY